High-luminosity primary vertex selection in top-quark studies using the Collider Detector at Fermilab

Adrian Buzatu

Master of Science

Department of Physics

McGill University

Montréal, Québec

August 2006

A thesis submitted to McGill University in partial fulfilment
of the requirements of the degree of Master of Science

Your file Votre référence
ISBN: 978-0-494-32676-3
Our file Notre référence
ISBN: 978-0-494-32676-3

Dedication

To Life. It always goes on.

Acknowledgements

This work could not have been possible without the direct and indirect support I received from teachers, colleagues, researchers, staff, funding agencies, doctors and friends.

I am in debt to my physics high school teacher back in Romania, Stefan Brinzan, who triggered my Physics enthusiasm through his clear lectures and relentless emphasis on the importance of asking questions, understanding the historical evolution of physics and balancing intellectual performance with sport. I am grateful to Jean-Yves Hostachy from LPCS, Grenoble, France and Takao Inagaki from KEK, Tsukuba, Japan for my first contacts with particle physics during my pre-graduate internships.

Once I started my graduate studies at McGill University, Montréal, Canada, as part of the CDF Collaboration at Fermilab, near Chicago, IL, USA, I found a very warm, supportive and friendly atmosphere both in the McGill University Physics Department and in the CDF Collaboration. This work is part of a large group effort and could not have been produced without the collective efforts of scientists and staff from McGill, CDF and Fermilab who keep the scientific infrastructure up and running.

I could not thank enough my supervisor, Andreas Warburton. He set an example of scientific and human professionalism that is worth following. I benefited from the friendly atmosphere he created in our research group. His feedback always prompt and constructive allowed me to improve. I owe him most of the particle physics skills that I developed so far. His financial efforts allowed me to spend time at Fermilab and conferences which helped me learn more and integrate in the particle physics scientific community.

I am grateful to Rob Snihur for his continuous prompt feedback and suggestions for our analysis. I am in debt to Jason Nielsen who guided my first steps through this analysis. I

acknowledge many useful discussions with CDF Collaborators, especially members of CDF IPP Canada and CDF top-quark properties subgroup.

I appreciate Camille Belanger-Champagne for reading a draft of my thesis and helping me improve its wording.

However, this dissertation would not have been possible if it were not for the efforts of some doctors and physiotherapists who helped me recover after a major accident that I suffered one month after I had started graduate school. Having recovered so well allowed me to do scientific research and outreach activities and to submit this thesis as scheduled initially despite three months I spent in hospital. Coming back to life represents my most important accomplishment during my MSc graduate studies.

I acknowledge I received direct financial support from the McGill University Department of Physics through its Teaching Assistantship and international fee weaver and from the National Science and Engineering Research Council of Canada (NSERC) through its Research Assistantship. We thank the Fermilab staff and the technical staffs of the participating institutions for their vital contributions. This work was supported by the U.S. Department of Energy and National Science Foundation; the Italian Istituto Nazionale di Fisica Nucleare; the Ministry of Education, Culture, Sports, Science and Technology of Japan; the Natural Sciences and Engineering Research Council of Canada; the National Science Council of the Republic of China; the Swiss National Science Foundation; the A.P. Sloan Foundation; the Bundesministerium fuer Bildung und Forschung, Germany; the Korean Science and Engineering Foundation and the Korean Research Foundation; the Particle Physics and Astronomy Research Council and the Royal Society, UK; the Russian Foundation for Basic Research; the Comision Interministerial de Ciencia y Tecnologia, Spain; in part by the European Community's Human Potential Programme under contract HPRN-CT-2002- 00292; and the Academy of Finland.

Abstract

Improving our ability to identify the top quark pair ($t\bar{t}$) primary vertex (PV) on an event-by-event basis is essential for many analyses in the lepton-plus-jets channel performed by the Collider Detector at Fermilab (CDF) Collaboration. We compare the algorithm currently used by CDF (A1) with another algorithm (A2) using Monte Carlo simulation at high instantaneous luminosities. We confirm that A1 is more efficient than A2 at selecting the $t\bar{t}$ PV at all PV multiplicities, both with efficiencies larger than 99%. Event selection rejects events with a distance larger than 5 cm along the proton beam between the the $t\bar{t}$ PV and the charged lepton. We find flat distributions for the signal over background significance of this cut for all cut values larger than 1 cm, for all PV multiplicities and for both algorithms. We conclude that any cut value larger than 1 cm is acceptable for both algorithms under the Tevatron's expected instantaneous luminosity improvements.

Abrégé

Il est essentiel pour beaucoup d'analyses au "Collider Detector" de Fermilab (CDF) de maximiser notre habilité d'identifier pour chaque collision de paquets de protons et antiprotons le vertex primaire (VP) appartenant à l'interaction forte qui produit une paire de quarks "top" ($t\bar{t}$) dans le mode "lepton et jets". On compare l'algorithme utilisé couramment par CDF (A1) à un autre algorithme (A2) en utilisant des simulations Monte Carlo à de grandes luminosités instantanées. On confirme que A1 est plus efficace que A2 à sélectionner les VPs d'une paire $t\bar{t}$ pour toutes les multiplicités de VP, les deux algorithmes ayant néanmoins des efficacités supérieures à 99%. La sélection des événements rejette des événements pour lesquels la distance le long du faisceau des protons entre le VP d'une paire $t\bar{t}$ et le lepton chargé (Δz) est plus grande que 5 cm. Les distributions d'une variable de discrimination entre le signal et le bruit en fonction de Δz sont quasi-constantes pour toute $\Delta z \geq 1$ cm pour les deux algorithmes et toutes les multiplicités de VP. On conclut que toutes les valeurs $\Delta z \geq 1$ cm est acceptable pour les deux algorithmes et les luminosités instantanées croissantes attendues pour le Tevatron.

Table of Contents

List of Tables

List of Figures

CHAPTER 1
Introduction

What is the Universe made of? What is matter made of? How does matter interact with matter? Why do things happen the way they do? The first to attempt to answer these questions were the Greek philosophers in Antiquity. Their best guess was that the Universe is made up of four elements: earth, water, fire and air. Almost four centuries ago, modern science started addressing these questions using both experimental and theoretical approaches. The scientific method proved to be very successful at answering questions about the Universe. This is how scientists learned that the Greeks had the right intuition, but the wrong elements.

It is our current understanding that matter has a granular structure and is made up of constituents which are made up of even smaller constituents. Matter is made up of molecules. Molecules are made up of atoms. Atoms are made up of nuclei and electrons. Nuclei are made up of protons and neutrons (nucleons). Nucleons are made up of quarks. We currently believe that electrons and quarks have no structure and are indivisible fundamental particles. New fundamental particles were postulated in order to explain the structure of hundreds of new particles discovered in the 1960s. The current paradigm states that ordinary matter is made up of six types of leptons and six types of quarks. Quarks and leptons interact with each other through four fundamental forces. Each force is carried by one or more types of gauge bosons. Cosmology revealed about a decade ago that ordinary matter represents on the order of only 4% of the energy content of the Universe, while the remaining constituents are dark matter (22%) and dark energy (74%).

Particle physics started out as a branch of nuclear physics in the 1950s, but it represents today an independent branch of physics. Particle physics is also called high energy physics and subatomic physics.

Particle physics presents two major domains. Accelerator-based particle physics uses beams of protons, antiprotons, electrons and/or positrons accelerated at very high energies by human made accelerators, either linear or circular. Accelerator-based particle physics operates two major types of experiments. In collider experiments two beams are collided against each other. In fixed target experiments a beam of particles is sent upon a fixed target. Cosmic-ray particle physics studies particles coming from outer space. These particles have the advantage of being much more energetic than those accelerated by humans and the disadvantage of having energies that cannot be chosen by humans in order to reproduce their experiments. As cosmic-ray particle physics experiments present low event rate and have therefore low statistics, collider physics is essential for studying particle physics. These particles typically collide with the atmospheric particles and create atmospheric particle showers. In all cases detectors identify and study final state particles created in collisions of initial state particles. Properties of particles and their interactions with other particles are thus studied.

1.1 The Standard Model

The current theory that explains with a great precision all the current data from particle physics is called the Standard Model. Reviews of the SM can be found in Ref. [1]and [2]. The SM is a quantum field theory based on the gauge symmetry groups $SU(3)_C \times SU(2)_L \times U(1)_Y$ [3]. $SU(3)_C$ describes the strong interaction, through Quantum Chromodynamics (QCD). $SU(2)_L \times U(1)_Y$ represents the electroweak interaction, which is spontaneously broken [4] into a weak interaction described by the V-A theory and an electromagnetic interaction described by Quantum Electrodynamics (QED). At current probing energies, gravity is very weak compared to these three forces. Therefore gravity can be ignored when describing fundamental particles at current energies. However, at probing energies on the order of the Planck scale [5], all four

forces may need to be explained by one theory, as gravity becomes as strong as the other three forces and cannot be neglected. String theory seems the current best theoretical candidate for unifying the four fundamental forces [3] [6].

The $SU(3)_C \times SU(2)_L \times U(1)_Y$ structure of the SM describes only interactions of massless particles. In order to create a theory that also accommodates massive particles, as we know they exist in reality, a spontaneous symmetry breaking mechanism called the Higgs mechanism is added to the SM. The Higgs mechanism [7] [8] [9] proposes that each fundamental particle acquires a mass proportional to its coupling to the Higgs boson, which is a spin-0 scalar field. At the time of submission of this thesis, the Higgs boson remains the last fundamental particle predicted by the SM that has not yet been observed. It is to be remarked, however, that the Higgs boson, if discovered, would be the first scalar field discovered ever.

New physics phenomena are expected to happen at the 1 TeV [10] probing energy scale. A series of models of physics beyond the SM have been developed. The most famous model in the context of supersymmetry is the minimal supersymmetric model (MSSM). This model predicts not one, but five Higgs bosons [11] [12], as well as weakly interacting massive particles (WIMPs [13]) as candidates for dark matter [14].

The Large Hadron Collider will start taking proton-proton collision data in 2008 at CERN, Switzerland. Its main goals are either to discover or to rule out the existence of the Higgs boson [9] and to search for physics beyond the SM, such as existence of supersymmetric particles or WIMPs or new mechanisms of spontaneous symmetry breaking [15] [16]. New information from new data would take us closer to the truth about Nature.

1.1.1 Fundamental Interactions

Any two electrically charged fundamental particles can interact through the electromagnetic force through an exchange of a massless photon (γ). Any two leptons can interact through the weak force through an exchange of a massive Z^0, W^+ or W^- boson. At high energies these two interactions merge into only one interaction, while their neutral carriers γ and Z^0 appear as

identical particles. Nevertheless, at low energies, they are clearly different particles as the photon is massless and the Z^0 boson is massive ($m_Z = 91.1876 \pm 0.0021$ GeV/c^2 [28]). This unique behaviour of two particles at high probing energies and distinct behaviour at low energies is an example of Spontaneous Symmetry Breaking [4]. Any two quarks can interact through the strong force through an exchange of a gluon that carries both colours of the interacting quarks. The colour charge is a quantum number particular to the QCD interaction in the same way as the electric charge is particular to the QED interaction. Because gluon-gluon interactions exist and photon-photon or Z^0-Z^0 or photon-Z^0 interactions do not exist, the strong force presents two properties not present in the case of the electromagnetic and weak forces. The first property, the colour confinement, states that all observed particles should be a colour singlet. A single gluon or quark may not exist by itself since it has a colour quantum number and only colour singlet particles may exist. This is why quarks may exist in pairs of quark-antiquark (mesons) or three quarks (baryons). Other combination of quarks have not yet been observed, even if they are allowed by the SM. Gluons may exist in groups called glueballs [17]. Glueballs have not yet been observed experimentally either. For quarks further apart than 1 fm, a confinement potential is modeled by $V(r) \approx \lambda r$, where $\lambda \approx 1$ GeV fm^{-1}. Trying to split apart a quark bound state needs a lot of energy that is used to extract pairs of particles and antiparticles from the vacuum. In this way a quark creates a jet of particles of particles in a process called hadronization.

The second property, asymptotic freedom, states that for quarks closer than 1 fm, the interaction strength decreases until only the leading order (LO) one gluon exchange dominates and the interaction potential can be modeled by $V(r) \approx -\frac{4}{3}\frac{\alpha_s}{r}$, where α_s is the strong coupling constant. For distances smaller than 1 fm, LO Feynman diagrams dominate and pertubative QCD calculations [18] are successful. At distances larger than 1 fm, higher order Feynman diagrams appear. In these cases, gauge lattice QCD calculations [19] [20] using discrete space

and time and demanding huge computing capacities are necessary. A review of the QCD interaction can be found in Ref. [21].

1.1.2 Fundamental Particles

There are two types of fundamental particles in the SM. Regular matter particles have semi-integer spin and are called fermions. They come in two types: leptons and quarks. Carriers of fundamental interactions have integer spin and are called bosons. Charge conjugation transforms every particle into its antiparticle, noted with a bar over its symbol. Antiparticles have the same mass, lifetime, decay width and spin as the particles, but have oppositely signed quantum numbers. The photon and the Z^0 boson are their own antiparticles.

There are six known types of leptons, which come in three weak isospin doublets, also called generations. The components of each generation are a lepton charged electrically with the electron electric charge and an electrically neutral lepton called a neutrino. The matter generations of leptons are (electron, electron neutrino) or (e^-, ν_e), (muon, muon neutrino) or (μ^-, ν_μ) and (tau, tau neutrino) or (τ^-, ν_τ). The antimatter generations of leptons are (antielectron, electron antineutrino) or (e^+, $\bar{\nu_e}$), (antimuon, muon antineutrino) or (μ^+, $\bar{\nu_\mu}$) and (antitau, tau antineutrino) or (τ^+, $\bar{\nu_\tau}$). Leptons interact only through electromagnetic and weak interactions.

There are also six known types of quarks. Each generation comprises one positively charged quark with two thirds of the electric charge of the electron and one negatively charged quark with one third of the electric charge of the electron. The matter generations of quarks are (up, down) or (u, d), (charm, strange) or (c, s) and (top, bottom) or (t, b).The antimatter families of quarks are (antiup, antidown) or ($\bar{u}$, $\bar{d}$), (anticharm, antistrange) or ($\bar{c}$, $\bar{s}$) and (antitop, antibottom) or ($\bar{t}$, $\bar{b}$). Quarks interact through electromagnetic and weak interactions, as leptons do, but also through the strong interaction thanks to the colour charge quantum number they possess (red, green or blue).

Throughout this thesis, unless otherwise mentioned, statements referring to particles are also true when referring to their antiparticles. For instance, electron designates both electron and positron. Table 1–1 presents a summary of the fundamental particles of the Standard Model and their properties.

Table 1–1: Standard Model fundamental particles and their properties.

Fermions	1^{st} Gen.	2^{nd} Gen.	3^{rd} Gen.	Interaction(s)	Electric Charge	Spin
Leptons	e^-	μ^-	τ^-	EM, Weak	-1	1/2
	ν_e	ν_μ	ν_τ	Weak	0	1/2
Quarks	u	c	t	EM, Weak, Strong	+2/3	1/2
	d	s	b	EM, Weak, Strong	-1/3	1/2
	Name	Force	Coupling	Mass (GeV/c^2)	Electric Charge	Spin
Gauge	γ	EM	10^{-2}	0	0	1
Bosons	W	Weak	10^{-13}	80.4	± 1	1
	Z	Weak	10^{-13}	91.2	0	1
	g	Strong	1	0	0	1

1.2 The Sixth Quark

The top quark is the most massive fundamental particle discovered so far. Its properties and phenomenology are presented in depth in various top-quark review articles [22] [23] [24] [25] [26] [27]. The particle Data Group lists the mass of the top quark as $m_t = 174.3 \pm 5.1$ GeV/c^2 [28] when measured directly from top-quark events and $m_t = 178.1^{+10.4}_{-8.3}$ GeV/c^2 when measured indirectly from the SM Electroweak fit.

The top-quark mass is about 35 times larger than that of the next most massive quark, namely the bottom quark, as $m_b = 4.6$ to 4.9 GeV/c^2 [28]. The top-quark mass is about five orders of magnitude larger than the masses of the lightest quarks that enter in the composition of regular atomic nuclei, such as the up quark ($m_u = 1.5$ to 4 GeV/c^2 [28]) and the down quark ($m_d = 4$ to 8 GeV/c^2 [28]). Fig. 1–1 presents the relative masses of the six types of quarks. The top-quark mass is about 175 times larger than that of a proton ($m_p = 938.27203 \pm 0.00008$ MeV/c^2 [28]). In more intuitive terms, the top-quark mass is approximately equal to the mass of a gold atom [28].

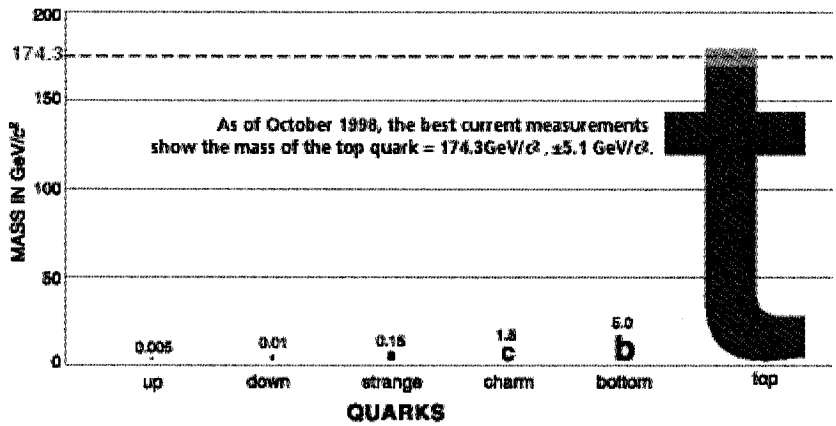

Figure 1–1: Relative mass of the six quarks

The top-quark mass is about twice the mass of the Z boson $m_Z = 91.1876 \pm 0.0021$ GeV/c^2 [28] and the W boson $m_W = 80.425 \pm 0.038$ GeV/c^2 [28]. Furthermore, the top-quark mass is comparable with the electroweak energy scale [29]. Also, the Yukawa coupling of the top quark

is almost one. All these point out that the top quark may play a role in the spontaneous symmetry breaking in models beyond the SM.

The top-quark mass is a free parameter in the SM and is a dominant parameter in higher order radiative corrections for several SM observables. The experimental uncertainty on the top-quark mass enters thus in the theoretical uncertainties of many SM quantitative predictions. However, the relative uncertainty on the top mass is the smallest among all fermions because of the very large value of the top-quark mass. Moreover, the top-quark mass and the W boson mass values constrain the mass of the Higgs boson (Fig. 1–2).

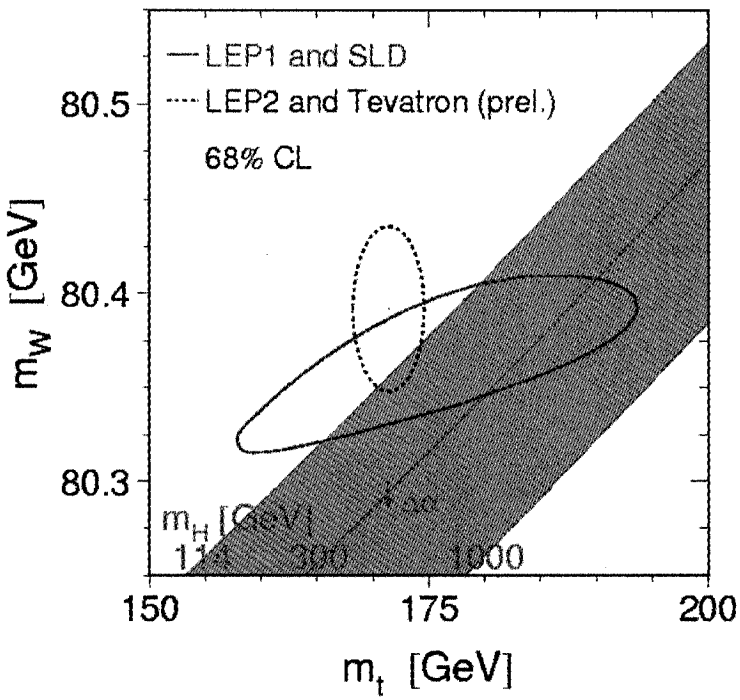

Figure 1–2: Higgs boson mass constraint from the top-quark mass and the W boson mass.

It is for these reasons that particle physicists are strongly motivated to measure the top-quark mass as precisely as possible. An uncertainty of 1 GeV/c^2 (compared to currently 1 GeV/c^2) would be ideal after collisions stop at the Tevatron in 2009.

1.2.1 Discovery

The first third-generation fundamental particle was discovered in 1977 at Fermilab [30]. This particle was called the bottom quark. An isospin partner for the bottom quark was proposed theoretically. The new particle, the top quark, was long searched for. Evidence for the existence of the top quark was published only in 1994 by the Collider Detector at Fermilab Collaboration (CDF) [31] [32]. The top quark was discovered one year later by both the CDF [33] and the DZero [34] Collaborations in proton-antiproton collisions from Run I of the Tevatron syncrothron accelerator at Fermilab at a center-of-mass energy of $\sqrt{s} = 1.8$ TeV. About a hundred events having a total integrated luminosity on the order of 100 pb^{-1} were enough to claim the long awaited discovery of the top quark.

Since 2001, both experiments have been taking data in Run II and have gathered more than 1 fb^{-1} of data up to the submission of this thesis. Many properties of the top quark have been observed and all the performed measurements agree with the SM predictions. Various analyses both at CDF and Dzero measure many properties of the top quark, such as the top-quark mass, the top-quark pair production cross section, the helicity asymmetry, the electric charge, possible top-quark production through a resonance and single top production [35].

1.2.2 Production

The SM allows the top quark to be produced either with (top-quark $t\bar{t}$ pair production) or without (single top-quark production) another top antiquark. Pair production is achieved through a strong interaction mediated by a gluon. Single top production is achieved through a weak interaction mediated by a W boson. Single top production has not yet been observed experimentally, but extensive searches are performed both at CDF and DZero. Pair production (Fig. 1–3) can be obtained either by quark-antiquark fusion and gluon-gluon fusion. The

relative importance of the two channels is a function of the center-of-mass energy ($\sqrt{s}$) and the types of the colliding particles. At the Tevatron, at a $\sqrt{s} = 1.96$ TeV, $t\bar{t}$ pair production happens in 85% of cases through quark-antiquark fusion and in 15% of cases through gluon-gluon fusion. The total $t\bar{t}$ production cross section obtained from CDF measurements using an integrated luminosity of 760 pb^{-1} of data is $\sigma = 7.4 \pm 0.5 \pm 0.6 \pm 0.4\ pb$ [35], where the respective uncertainties are statistical, systematic and originating from luminosity measurements. A good review for theoretical predictions of the top-quark cross section can be found in Ref. [36]. Top pair production is a very rare process, since on average only one inelastic collision in 10^{10} produces a $t\bar{t}$ pair. However, at the proton-proton collisions at the center-of-mass energy of $\sqrt{s} = 14$ TeV at the Large Hadron Collider (LHC), gluon-gluon fusion will dominate the top pair production mechanisms and the total $t\bar{t}$ pair production cross section will be considerably larger than at the Tevatron [36].

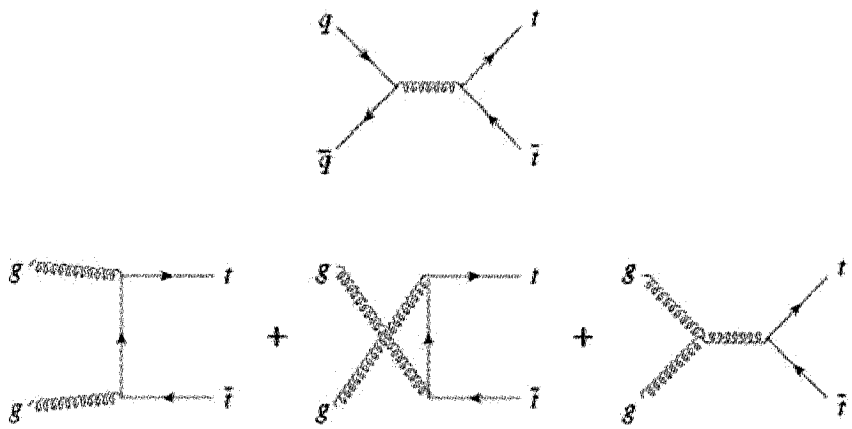

Figure 1–3: Feynman diagrams for top-quark pair production

Intensive searches at CDF and DZero are dedicated to single top-quark production. If single top-quark production is observed experimentally, the CKM matrix element $|V_{tb}|^2$ [37] can be measured. As the single top-quark production cross section is proportional to this CKM matrix element, σ can also be measured. A single top production cross section larger than its SM predicted value could be a sign of new physics beyond the SM. Moreover, single top

production is expected to represent the largest irreducible background for some Higgs searches at the LHC.

1.2.3 Decay

A top-quark decays in a time interval $\tau = 3 \cdot 10^{-25}\ s$ [22] shorter than the hadronization time $\tau = 25 \cdot 10^{-25}\ s$ [22]. This is why the top quark cannot form bound states of hadrons and it can be studied only through its decay products. A top quark decays almost 100% of the time to a W^+ boson and a bottom (b) quark. An antitop antiquark $\bar{t}$ decays almost 100% of the time in a W^- boson and an antibottom antiquark ($\bar{b}$) [22]. Since top-quark pairs are created and decay near the beam axis almost at rest due to the large top-quark mass, the primary vertex created by the $t\bar{t}$ pair decay is very close to the beamline. The top-quark pair decays into two W bosons and two b quarks. Any quark other than a top quark becomes a jet through the process of hadronization described earlier. A W boson can decay either leptonically, to a lepton and a neutrino, or hadronically, to a quark-antiquark pair. There are three top-quark pair decay channels, each with its own signatures.

In the dilepton channel both W bosons decay leptonically. The final state particles are two charged leptons of opposite charge, two neutrinos and two b quarks. The signature of the dilepton channel is formed by two charged leptons of opposite charge, large missing transverse energy and two jets, both originating from b quarks.

The lepton-plus-jets channel is studied in this dissertation. In this channel, one W boson decays leptonically and the second W boson decays hadronically. The final state particles are one charged lepton, one neutrino and four quarks (two originating from b quarks). The signature of the lepton-plus-jets channel is formed by z X one charged lepton, large missing transverse energy and four jets, two of them originating from b quarks.

In the all-hadronic channel both W bosons decay hadronically. The final state particles are six quarks, two of them b quarks. Its signature is therefore six jets, two of them originating from b quarks.

The dilepton channel is a relatively clean channel, having a relatively large signal over background (S/B) ratio, but presents a relatively low event rate. The lepton-plus-jets channel presents is less clean, having a smaller S/B ratio, but presents a relatively higher event rate. The all-hadronic channel is the least clean, presenting a lot of background and a smaller S/B ratio, but it presents the largest event rate and is the only channel that allows a full event reconstruction due to the lack of neutrino in the event signature. Fig. 1–4 presents the percentage distribution (Braching Ratios) of the top-quark pair decay channels and Fig. 1–5 presents the Feynman diagram of quark-quark fusion, top-quark pair production and a summary of all possible decay channels of the top-quark pair. Table 1–2 quantifies these qualitative statements.

.

Table 1–2: Comparison between top-quark pair decay channels

Comparison between top-quark pair decay channels, where "BR" means "Branching Ratio" and "Evt Rate" means "Event Rate/100 pb^{-1}".

Channel	BR (%)	S/B	Evt Rate	Fully reconstructed?
Dilepton	10	1.5-3.5	4-6	No
Lepton-plus-jets	44	0.3-3	25-45	No
All-hadronic	46	-	-	Yes

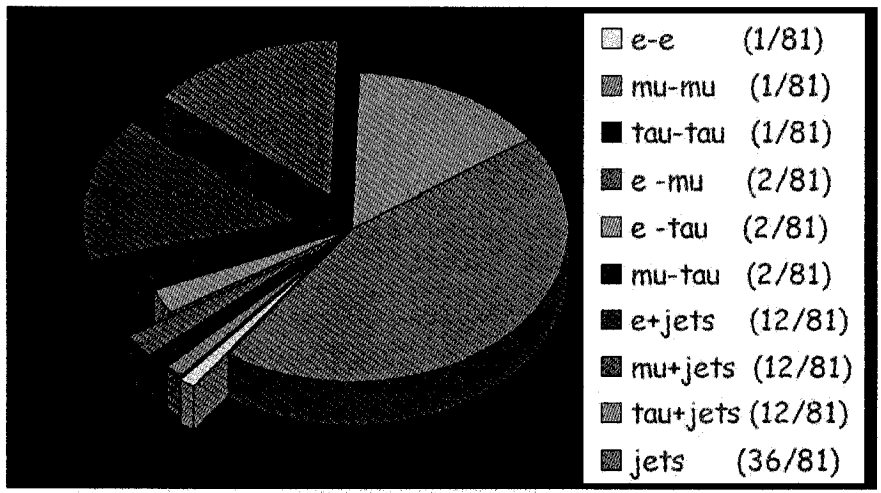

Figure 1–4: Percentage distribution of the top-quark pair decay channels.

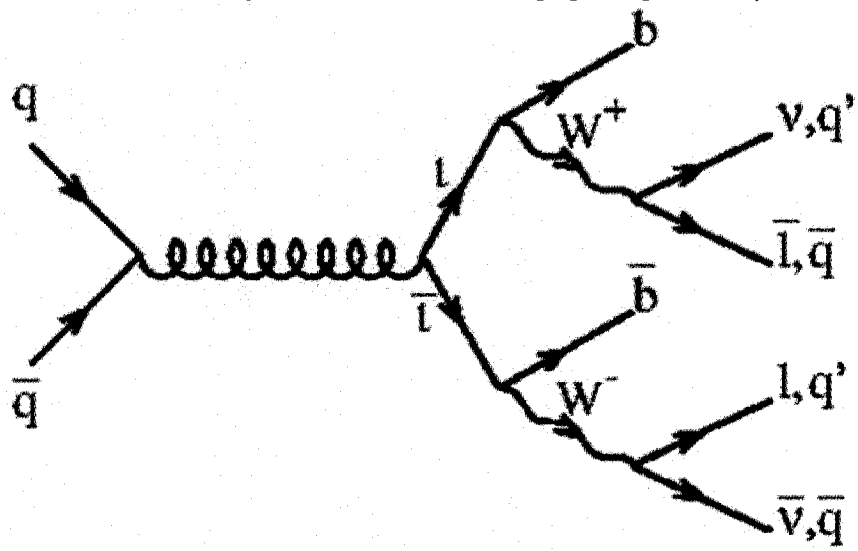

Figure 1–5: General Feynman diagram of $q\bar{q} \rightarrow t\bar{t}$ and subsequent decay.

CHAPTER 2

Experimental Infrastructure

Accelerator based particle physics examines final particles created in initial particle collisions. The most interesting processes have often very rare signatures. Counting experiments count the number of events where the particular signature appears; any excess above the estimated background is considered as signal. Per unit time, a signature occurs in a number of events proportional to the physical probability of occurrence (cross section σ) and to the beam collision conditions in the accelerator complex (instantaneous luminosity $\mathcal{L}$). However, not all events are reconstructed and identified by the particle physics detector. The experimental efficiency (ϵ) measures the percentage of events that are seen correctly by the detector. Therefore, the observed number of events is given by $N_{obs}/second = \epsilon \cdot \sigma \cdot \mathcal{L}$. Integrating the instantaneous luminosity obtains the integrated luminosity, which gives the total number of observed events $N_{obs} = \epsilon \cdot \sigma \cdot \int \mathcal{L}dt$.

Since the physical cross section of many processes increases with the center-of-mass energy ($\sqrt{s}$), particle physicists try to build accelerators with larger and larger $\sqrt{s}$. Furthermore, particle physicists try to build better detectors with reconstruction efficiencies for various particles very close to one.

The only particle accelerator and collider in the world that produces real top-quark pairs is the Fermilab $p\bar{p}$ Accelerator Complex, based in Batavia, Illinois, USA. Its main accelerator is called the Tevatron. Between 1992 and 1995, the Tevatron collided protons and antiprotons at $\sqrt{s} = 1.8$ TeV. This period is called Run I. Since 2001, the Tevatron operates at $\sqrt{s} = 1.96$ TeV. This period is called Run II and is estimated to end in 2009.

For $\sqrt{s} < 3\ TeV$, proton antiproton colliders are more advantageous than proton proton colliders to create quark antiquark final state particles, such as the top-quark pair studied in this dissertation. This is due to the parton distribution functions of protons and antiprotons. At small center-of-mass energies, valence quarks and gluons are dominated by the regular two quarks up and one quark down [38]. As $\sqrt{s}$ increases, gluons start dominating the content of protons and valence antiquarks come in non-negligible percentages. This is why, from 2008 on, the LHC will be very effective at producing top-quark pairs in proton-proton collisions at $\sqrt{s} = 14$ TeV.

When comparing $p\bar{p}$ and pp colliders from a technological point of view, the former have the advantage of requiring only a tube and one a magnetic field to accelerate both beams and the disadvantage of the difficulty of creation and storage of antiprotons. On the other hand, two sets of magnets in two rings are needed for the LHC, but protons are easy to produce and accelerate.

2.1 Minimum Bias Interactions

The trigger time window, opened during a bunch crossing, is called an event. An event may therefore contain more than one hard interaction (inelastic collisions), which typically originate from the annihilation of two partons from a proton and an antiproton. All hard interactions that are recordable without any special triggering criteria constitute what are called minimum bias events. Every hard interaction creates a primary interaction vertex (PV), the point from where all prompt particles emerge. Experimentally, prompt tracks originate from a PV and jets are clustered with respect to a PV. Usually the remaining partons of the top and antitop quarks (spectator partons) continue with the beam. Sometimes the spectator partons suffer a soft interaction (elastic collisions) where they are scattered at a small angle. This process is called underlying event. Since they also leave energy deposits in the detector, the underlying event also biases the measurements and it needs to be corrected for. Very rarely, underlying events may create their own PV if they are energetic enough. The number of PVs per event is

called PV multiplicity and it counts mostly hard interactions, but also a few soft interactions. The phenomenon where other signals are present in the time window of the searched for signal is called pile-up in more general terms.

Since the main focus of this dissertation is minimum bias interactions in bunch crossings where top-quark pairs in the lepton-plus-jets channel occur, it is helpful to enumerate the center-of-mass energy ($\sqrt{s}$), the bunch spacing (b.s.), the instantaneous luminosity ($\mathcal{L}$) and the average PV multiplicity per event($< n >$) encountered until now and expected in the future at the Tevatron (Tev) in Table 2–1. For comparison, the same variables are described also for the LHC environment.

Table 2–1: Performance of Tevatron and LHC

Parameter	Tev I	Tev II now	Tev II end	LHC start	LHC design
$\sqrt{s}$ (TeV)	1.8	1.96	1.96	14	14
b.s. (ns)	3500	396	396	40	40
$\mathcal{L}$ ($\cdot 10^{32} cm^{-2} s^{-1}$)	0.16	0.5	3	10	100
$< n >$	2.5	1.9	4-5	2-3	25

The PV multiplicity is given by the product of the instantaneous luminosity and the total cross section (number of events per unit of time) and the bunch crossing time, which can be considered the same as the bunch spacing. Therefore, $< n >= \mathcal{L} \cdot \sigma_{tot} \cdot b.c.$. Particle physicists desire to have the maximum number of hard interactions per unit of time ($\mathcal{L}$), but the minimum number of hard interactions in the same bunch crossing (minimum $< n >$). This goal is obtained by decreasing the bunch spacing, which in its turn requires very fast readout electronics and hardware triggers. We especially remark that Tevatron Run I, Tevatron Run II now and LHC in its first years all have about 2 PVs per event, increasing instantaneous luminosity and decreasing bunch spacing. The bunch spacing is fixed for the Run II at the Tevatron. To increase the data taken by CDF and DZero, the Tevatron increases its instantaneous luminosity in time, as seen in Fig. 2–1. This leads to an increase of hard interactions per event from 2 (now) to 4-5 (end).

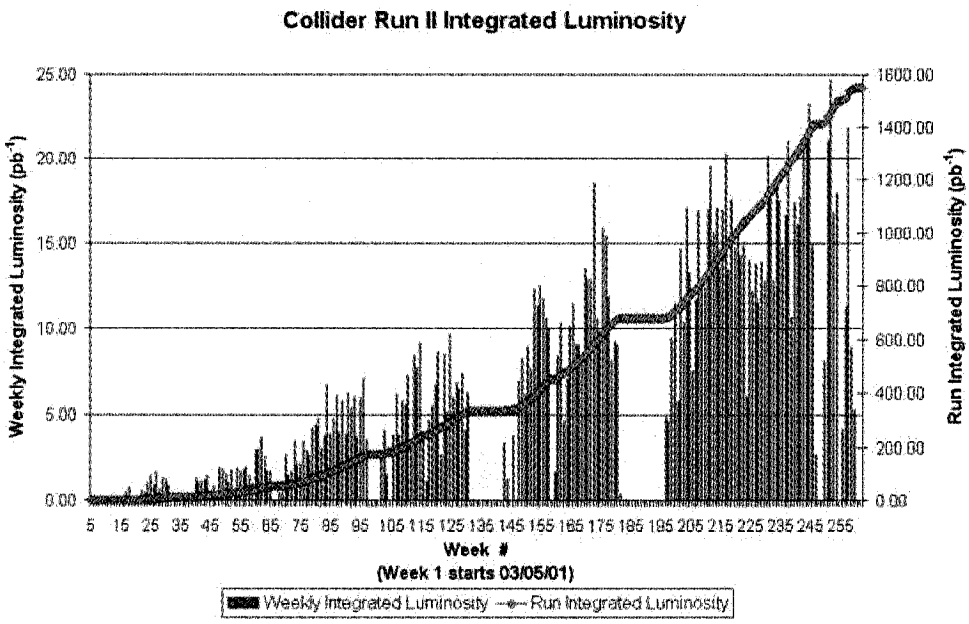

Figure 2–1: Increase of instantaneous luminosity with time at Tevatron Run II.

The Tevatron's instantaneous luminosity is given by $\mathcal{L} = \frac{fE}{\epsilon_n} \cdot \frac{n_b N_p N_{\bar{p}}}{\beta^*}$. The first fraction presents quantities that cannot be easily changed after the experiment is started, such as f, the beam revolution frequency at the Tevatron, which is set by the radius and the speed of light c; E, the beam energy set by the physics goals of the experiment; ϵ_n, the beam emittance at injection set by getting the beam into the Tevatron. The second fraction presents quantities that can be changed easily during the period of taking data, such as n_b, the number of proton or antiproton bunches found at one time in the Tevatron; β^*, the strength of the final focus; N_p ($N_{\bar{p}}$), the number of protons (antiprotons) per bunch.

2.2 Cherenkov Counters

It is crucial for this analysis to estimate the number of $p\bar{p}$ (primary) interactions on an event-by-event basis. This task is performed by the CDF Cherenkov Luminosity Monitor [41], located in the end-plug forward and backward calorimeters, in the pseudorapidity range $3.7 < |\eta| < 4.7$. There are three layers of Cherenkov counters concentric around the beamline, pointing toward the interaction region. Each layer contains 16 Cherenkov counters that are conical, and filled with isobutane gas at atmospheric pressure. The choice of the gas radiator was motivated by its large index of refraction ($n = 1.00143$) and its good transparency for ultra-violet photons, where most of the Cherenkov light is emitted. For this choice of gas, the Cherenkov light cone half-angle is $\theta_c = 3.1°$; the momentum threshold for light to be emitted is 9.3 MeV/c for electrons and 2.6 GeV/c for pions.

Particles produced in primary interactions cross the full Cherenkov counter and produce a large signal of about 100 photoelectrons. Particles produced in other interactions, such as in those between particles of the beam and particles of the beam pipe, produce smaller photoelectron yields. Once the instantaneous luminosity is estimated, it is used by the CDF control room to monitor the collider performance and by the CDF data acquisition system to

monitor the system triggers and the trigger rates. Asynchronously, the instantaneous luminosity is also added to the CDF data, for the offline analysis.

2.3 The Fermilab $p\bar{p}$ Accelerator Complex

Fig. 2–2 (2–3) represents a bird's eye (schematic) view of the Fermilab $p\bar{p}$ Accelerator Complex.

When 36 new bunches of protons and 36 new bunches of antiprotons enter the Tevatron, it is said that a new store starts. A typical bunch length is 0.43 meters. Both beams have an average energy per accelerated particle of 980 GeV. A proton bunch contains typically $3.30 \cdot 10^{11}$ protons. An antiproton bunch contains typically $3.60 \cdot 10^{10}$ antiprotons. Since antiprotons are antimatter, they annihilate with regular matter. This is why antiprotons are accumulated about one order of magnitude less than protons. As the two beams collide head on at a rate of 2.5 million times per second, hard scatterings occur at a certain rate per unit of time, which is described by the instantaneous luminosity. As the store's duration increases, instantaneous luminosity decreases exponentially. Typically after 24 hours the proton and antiproton bunches are evacuated from the Tevatron and subsequently new bunches are inserted in the Tevatron and a new store starts. Stores may end prematurely when the beam is lost in a process called quenching. Quenches may happen when a beam hits a superconducting magnet. The magnet is locally not superconducting any more and releases energy by Joule effect [39]. Soon the whole magnet warms up and is no longer superconducting. Physicists then need for the whole magnet to be cooled down in liquid helium before inserting a new store in the Tevatron. A typical integrated luminosity per week is $\int Ldt = 8\ pb^{-1}$.

Acceleration of protons and antiprotons to collision energies is realized by a complex of eight accelerators, two linear (Cockcroft-Walton and Linac) and six circular synchrotrons (Booster, Main Injector, Debuncher, Accumulator, Recycler and Tevatron). This huge accelerator complex consumes 30 MW of electric power and stretches over 9 km.

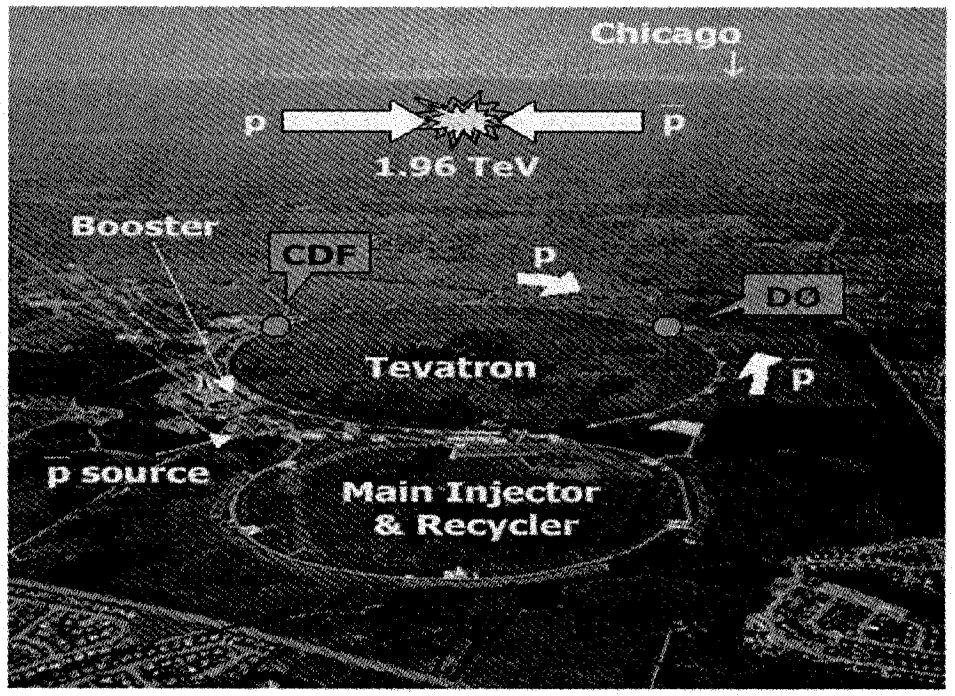

Figure 2–2: Bird's Eye View of the Fermilab $p\bar{p}$ Accelerator Complex

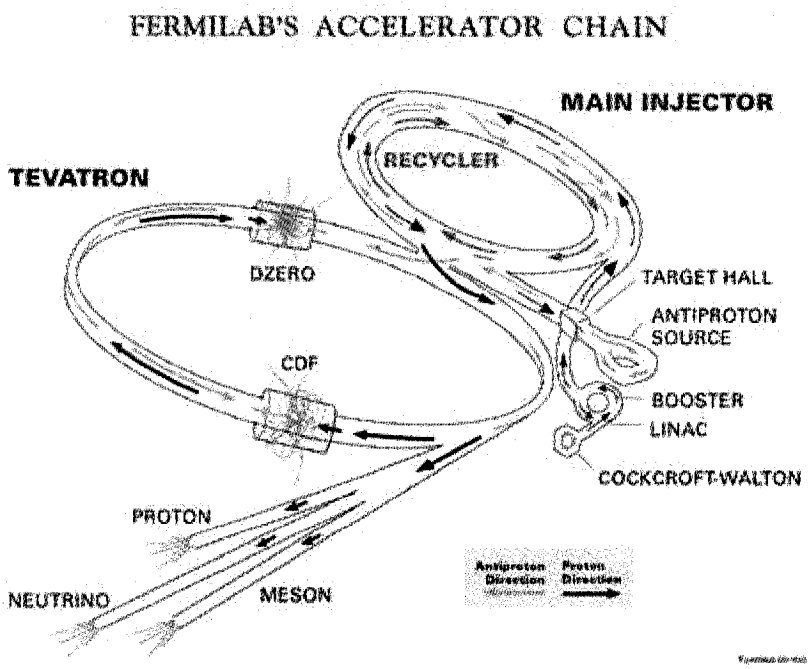

Figure 2–3: Schematic view of the Fermilab $p\bar{p}$ Accelerator Complex

2.3.1 Protons

First, protons have to be produced. A strong electric field ionizes hydrogen atoms at room temperature (0.04 eV/atom) and sends protons and electrons in opposite directions. The protons fall on and stick to a cesium surface. The work needed to free an electron from a cesium surface is smaller than in the case of any other atom, since cesium is the most reactive atom. A falling atom may collide with a group consisting of a proton and two electrons that are temporally together on the cesium surface. The group is thus freed from the surface and it forms a hybrid negative hydrogen ion (H^-). Thanks to the same electric field, a continuous beam of H^- of about 25 keV is collected.

The beam is accelerated by a Cockcroft-Walton accelerator to an energy of 750 keV by a constant electric field. The acceleration voltage is limited by the fact that at high voltages the air creates sparks.

The beam is subsequently accelerated to 400 MeV by a 130 m long linear accelerator called the Linac. The Linac uses alternative current and resonant frequency cavity technology. The continuous beam is therefore bunched up. When outside a cavity, a bunch is accelerated by an electric field. When inside a cavity, a bunch does not see the electric field now in the opposite direction and therefore is not decelerated. As particles acquire momentum, cavities and gaps are longer to provide constant acceleration. A typical bunch has $1.5 \cdot 10^9$ particles. A typical bunch distance is 4ns. A typical pulse contains 4,000 bunches, a total of $6 \cdot 10^{12}$ particles and a typical pulse length of 20 ms. While in the Linac, a particle is accelerated by an electric field of 3MV/m. The beam power is 18 MW when the pulsed hybrid H^- ion beam exits the Linac.

To strip both electrons away, the beam is passed through a carbon foil. The proton beam is injected into a 475 m circumference circular synchrotron accelerator called the Booster. A synchrotron accelerates charged particles thanks to a resonant frequency cavity. As their momentum increases, particles are kept at a constant radius by a corresponding increase of the magnetic field. The proton beam is accelerated every turn by a 500 kV voltage drop. After

completing 16,000 turns in 33 ms, the beam has 8 GeV, exits the Booster and enters the Main Injector synchrotron accelerator. Protons of 150 GeV are injected in the Tevatron synchrotron accelerator.

2.3.2 Antiprotons

Antiproton production occurs in the antiproton source. The bunched beam of 120 GeV protons from the Main injector smashes on a 7 cm nickel target every 1.5 s. Particles created in the forward direction are recovered through a lithium lens. A pulsed magnet acting as a charge-mass spectrometer selects only antiprotons. The antiproton beam is pulsed, which means the beam exhibits a large energy spread and a small time spread. To be debunched, the beam is passed into another synchrotron accelerator, called the Debuncher. Low (high) energy antiprotons follow the interior (exterior) path, arrive at different times at the resonance frequency cavity. As they see different phases, low (high) energy antiprotons are accelerated (decelerated). After about 100 ms, the antiproton beam is almost continuous, having a small energy spread and a large time spread. After 1.5 seconds in the Debuncher, the beam is injected into yet another circular synchrotron, called the Accumulator. A new pulsed antiproton beam is then inserted into the Debuncher. It takes 1 million 120 GeV protons to hit the nickel target for 20 8 GeV antiprotons to be injected into the Accumulator.

The Accumulator uses stochastic cooling to accumulate antiprotons while keeping them at the desired (very small) longitudinal (transverse) momentum for hours, even days. The Accumulator has a shape of a triangle with rounded corners. Stochastic cooling transforms particles from a hot state, with large spreads in energy, to a cooler state, with smaller spreads in energy, thanks to a feedback technique using pickups and kickers [40]. Van der Meer received the Nobel Prize for stochastic cooling in 1984.

The continuous beam of 8 GeV antiprotons from the Accumulator is injected in the Main Injector. The Main Injector replaced in 1998 the Main Ring situated in the same tunnel as the Tevatron. This represents one of the major upgrades from Run I to Run II. The Main Injector

accelerates both protons and antiprotons in the same ring, using the same magnetic field. 150 GeV antiprotons are sent in the Tevatron accelerator where they are accelerated to 980 GeV and collided with the proton beam. When a store ends, almost 75% of the antiprotons survive. Since creating antiprotons is such a hard task, surviving antiprotons are recuperated in another sychrotron accelerator, called the Recycler.

The Recycler sits just above the Main Injector and acts as a fixed-energy storage ring thanks to its permanent refrigerator-like magnets and stochastic cooling. The Recycler receives antiprotons both from the Accumulator and from the Tevatron at the end of a store. The Recycler acts as an antiproton storage ring until the Tevatron is ready to accept antiprotons in a new store.

2.3.3 The Tevatron

When built in 1983, the Tevatron was the first superconducting synchrotron accelerator. The Tevatron's 1000 superconducting electromagnets can produce a magnetic field as large as 4.2 Tesla. Electromagnet coils are made of 8 mm niobium-titanium alloy wire. One coil contains about 70,000 km of wire. A dipole magnet is about 6.4 m long. Once per turn, particles receive a kick in energy of about 650 kV from a resonance frequency cavity. In about 20 seconds the magnetic field increases gradually from 0.66 Tesla to 3.54 Tesla, while the beam energies increase gradually from 150 GeV to 800 GeV. Meanwhile, the beams turns around the 1 km radius circular accelerator 1 million times. When the beams arrive at 980 GeV, an electric current of more than 4 kA flows through the electromagnet and creates a magnetic field of 4.2 Tesla. For comparison, the superconducting magnets at LHC will run at 8.4 Tesla when the beam energy will be 7 TeV. Superconducting electromagnet coils kept at liquid helium temperature (4.3 K) have no resistance and therefore dissipate no energy through the Joule effect. Significantly larger currents are able to flow though these coils in order to produce very large magnetic fields. Tevatron's cryogenic system is the world largest. If it absorbs 23kW

of power, it can still maintain the liquid helium temperature. The system can deliver 1000 liters/hour of liquid helium at 4.2 K.

Table 2–2 summarizes the acceleration characteristics of the different stages of the Fermilab $p\bar{p}$ Accelerator Complex. In this table, $\beta = \frac{v}{c}$ expresses the speed of the particle as a fraction of the speed of light in the vacuum and $\gamma = \frac{E}{pc} = \frac{1}{\sqrt{1-(\frac{v}{c})^2}}$ is the relativistic factor. Also, for highly relativistic particles, kinetic and total energies can be approximated.

Table 2–2: Performance of Fermilab $p\bar{p}$ Accelerator Complex, where C-W=Cockwroft-Walton, L=Linac, B=Booster, Debuncher and Recycler, M=Main Injector, T=Tevatron, A=Accelerator, E=Energy

A.	H	H^-	C-W	L	B	M	T
E	0.04 eV	25 keV	750 keV	400 MeV	8 GeV	50 GeV	0.98 TeV
β	$9.1 \cdot 10^{-8}$	0.01	0.04	0.71	0.99	1	1
γ	1	1	1	1.43	9.53	161	1067

2.4 The Collider Detector at Fermilab

At two proton-antiproton collision points in the Tevatron, two detectors are installed in order to reconstruct the new particles created in these collisions. These detectors are the Collider Detector at Fermilab (CDF) and DZero. Each detector is operated by a collaboration of about 500 scientists. In this dissertation we will study events recorded by the CDF detector.

Because of its cylindrical symmetry, particles reconstructed by the CDF detector are described in a cylindrical system of coordinates: z is the direction of the proton beam; ϕ is the azimuthal angle; θ is the polar angle. However, the pseudorapidity quantity $\eta = -\ln\left[\tan\left(\frac{\theta}{2}\right)\right]$ is more convenient to use since the most interesting particles to be studied at CDF are high transverse momentum particles having θ close to 90° and η close to zero and since units of rapidity $\tan\frac{\theta}{2}$ have equal particle multiplicities at hadron colliders.

The CDF II detector has three main parts. The tracking systems are formed by the innermost layers of the detectors and measure very well the transverse momentum of electrically charged particles, while reconstructing tracks and vertices. The electromagnetic (hadronic) calorimeters measure the energy of a particle in a destructive way. A particle is transformed into a shower that is fully contained and measured by the calorimeters. As muons traverse the whole detector leaving almost no energy deposits, the most exterior layers are dedicated to to muon detection. Fig. 2–4 represents a schematic view of the CDF detector.

2.4.1 Tracking Systems

The tracking systems of CDF II use drift cell and silicon microstrip technology. A drift cell chamber (silicon detector) system offers good coverage in the detector region $|\eta| < 1.0$ ($|\eta| < 2.0$). Both systems are immersed in a 1.4 Tesla magnetic field parallel to the proton beam and created by a 5 m long and 3.2 m in diameter superconducting solenoid. Charged particle trajectories are curved by the magnetic field and the curvature radius is used to infer their transverse momentum (p_T). Therefore, the tracking systems are not sensitive to neutrally charged particles.

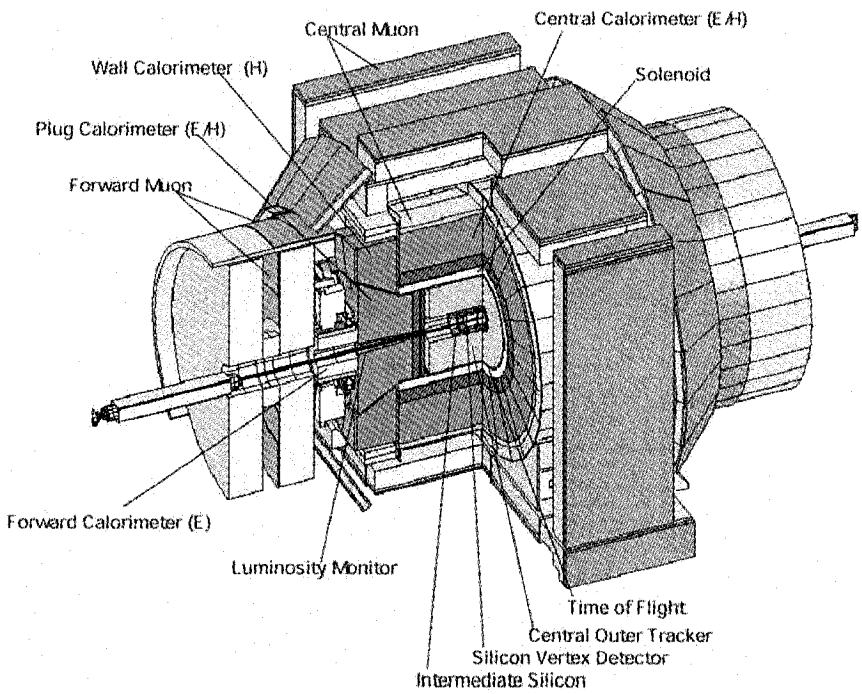

Figure 2–4: Schematic view of the CDF detector

The 3.1 m long drift cell chamber is called the Central Outer Tracker (COT). The COT covers the radial region between 0.40 m and 1.37 m measured from the beam axis. The COT has 96 different segments. In the COT 8 axial wires alternate with 8 sense wires. Stereo superlayers at $\pm 2°$ each having 12 wires give a third dimension coordinate for the particle hits. A single drift time measurement has a position resolution of 140 μm. The passage of a particle leaves a series of point hits, thus a series of line segments. Two complementary algorithms fit these lines to a circle and identify which axial hits belong to one charged particle. Once we have the two dimensional image, we merge the axial hit information with the stereo one in order to build a 3D image of the track. In this thesis we require at least 3 axial superlayer hits and 2 stereo superlayer hits. A superlayer is considered hit if it has 5 individual hits. In general, the p_T resolution for high p_T tracks scales like the p_T value ($\frac{\delta p_T}{p_T} = 0.1\% p_T(\text{GeV})$). The distance of minimum approach of the track to the beamline is called the impact parameter (d_0) and has a resolution of $\delta d_0 \approx 350 \mu m$. Muon trajectories are typically almost straight lines.

Five double-sided silicon layers form the silicon microstrip detector (SVX), which covers the radial region between 2.5 and 11 cm from the beamline. Three (two) of these layers perform r-ϕ measurements on one side and 90° (1.2°) stereo measurements on the other side. The SVX has a length of 96 cm and covers about 90% of the luminous region, the region where inelastic collisions take place. The average resolution of a silicon hit is 11 μm. Another silicon detector called the intermediate silicon layer (ISL) covers the radial region 19 to 30 cm. The ISL makes the connection between the tracks of the SVX and the COT. An outside-in tracking algorithm adds silicon hits to a reconstructed COT track, thus improving the track impact parameter resolution to 30 μm, including the beam position uncertainty.

Tracking information is also used in triggering thanks to a pattern recognition algorithm based on a hardware piece called the eXtremly Fast Tracker (XFT) that runs online. The XFT identifies track candidates with four matching axial hits on a given trajectory. Track

identification has an efficiency of $96.7 \pm 0.1\%$ for charged particles with $p_T > 25$ GeV/c. Fig. 2–5 represents a schematic view of the tracking system of the CDF detector.

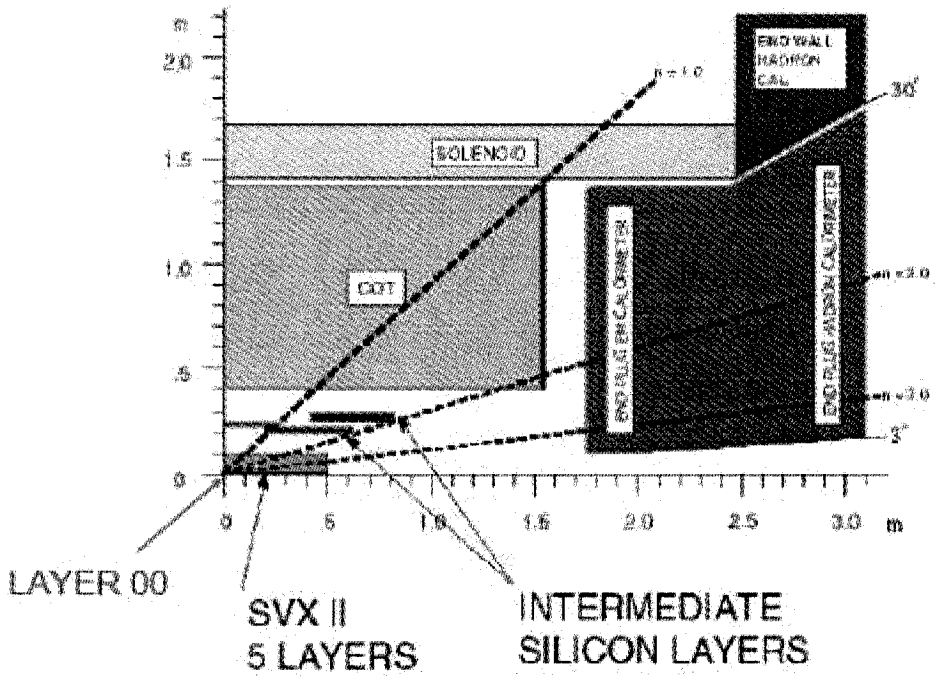

Figure 2–5: Schematic view of the tracking system of the CDF detector.

2.4.2 Calorimetry

The calorimeter systems are found outside the tracking systems and the solenoid in the radial direction. Based on projective geometry, the calorimeter systems contain both electromagnetic (EM) calorimeters that reconstructs electromagnetic showers and hadronic (HAD) calorimeters that reconstruct jets. EM showers are produced by electrons, positrons or photons. Electrons and positrons emit photons when accelerated (bremsstrahlung radiation) and photons convert to electron-positron pairs. The whole shower is typically contained in the EM calorimeter. The EM shower energy is considered the energy of the initial particle. Hadronic showers are produced by jets of hadrons that are created by the hadronization of quarks. Jets leave a small fraction of their energy in the EM calorimeter and a large fraction in the HAD

calorimeter. Muons leave calorimeter energy deposits consistent with minimum ionizing particles. Therefore, muons do not develop any type of shower. Fig. 2–6 represents symbolically how electrons, photons, muons and jets are seen in the calorimeter system.

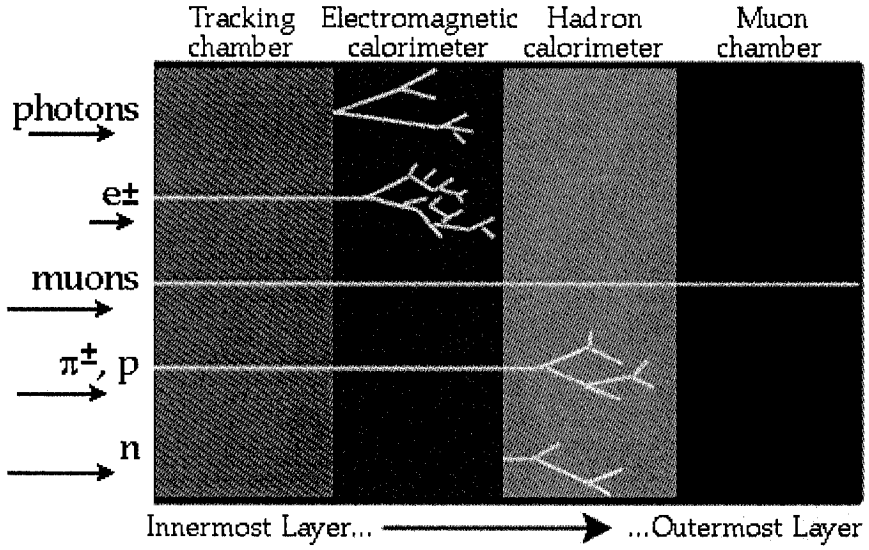

Figure 2–6: Particles in the CDF detector
Electrons, photons, muons and jets as seen in the calorimeter system

The EM calorimeters are lead-scintillator sampling detectors. The HAD calorimeters are iron-scintillator sampling detectors. Both calorimeters are made up of towers that occupy a certain region in η and ϕ. The calorimeter systems offer a $0 \geq \phi \leq 2\pi$ and $|\eta| < 3.6$ coverage. At the typical radius where EM showers reach their maximum, proportional and scintillating strip detectors called the CES detectors measure the shower transverse profile.

Energy measurements at hadron colliders are not beam constrained, as measurements at electron-positron colliders are. Due to parton distribution functions, the longitudinal momenta of annihilating partons are not precisely known. Transverse energy and momentum are therefore the relevant quantities to measure.

A typical energy deposit cluster is shared by a few neighboring towers. The calorimeter trigger system keeps a list of all clusters in the EM calorimeter for the electron/positron reconstruction and a list of all clusters, both EM and HAD calorimeter, for jet reconstruction

.

Both calorimeter detectors have barrel (central) and plug (forward) subsystems. Central electron candidates consist of an isolated cluster in the central EM detector that matches an XFT track in the pseudorapidity range $|\eta| < 1.1$. The energy resolution of a central electron candidate scales with the square root of the transverse energy: $\frac{\sigma(E_T)}{E_T} = \frac{13.5\%}{\sqrt{E_T(\mathrm{GeV})}} \oplus 2\%$. Since jets typically contain various particles, jet candidates are considered a multitude of both EM and HAD clusters that fall within a cone of radius $\Delta R = \sqrt{\Delta\phi^2 + \Delta\eta^2} \leq 0.4$. Measured jet energies need to be corrected for calorimeter nonlinearity, multiple primary interactions and energy losses in the gaps between the towers. The jet transverse energy resolution is given by $\frac{\sigma(E_T)}{E_T} = 0.1\left(\frac{E_T}{\mathrm{GeV}} + 0.1\right)$.

2.4.3 Muon Chambers

Muon candidates are reconstructed in drift chambers located outside the calorimeter systems. Just outside the calorimeter system there is a planar drift chamber made up of four layers (CMU) that is able to reconstruct muons with $p_T > 1.4$ GeV/c. Another drift chamber made up of four layers (CMP) that reconstructs muons with $p_T > 2.0$ GeV/c follows after 60 cm of steel. Although the two planar chambers have different structure and geometrical coverage, the CMU and CMP cover the $|\eta| < 0.6$ (central) region. In order to have coverage in the $0.6 < |\eta| < 1.0$ region, four layers of drift chambers called the CMX detector are also added and cover a conic section outside the central calorimeter. These three muon detectors span the full η region covered by the COT. Stubs in the CMU and CMP (CMX) muon detectors matched to a COT track are called CMUP (CMX) muon candidates.

2.4.4 Trigger Systems

The CDF detector uses a three-level trigger system. The trigger system is meant to select, every second, the most interesting 100 bunch crossings to examine from the 1.7 million that occurred. The first level trigger (L1) is performed by a very fast dedicated hardware that reduces the frequency from 1.7MHz to 25 kHz. L1 performs hardware tracking for $p_T > 1.5$ GeV, muon-track matching, electron-track matching, missing transverse energy and sum of transverse energy measurements. L1 uses 42 buffers. The second level trigger (L2) is performed by a hardware component and Linux computers. L2 uses four buffers and performs silicon tracking, jet finding and refined electron/photon finding. After L2, the frequency is reduced to 500. The third trigger level (L3) is performed by a farm of 200 Linux computers that perform full event reconstruction using an offline software charged-lepton selection identical to the one done in this analysis. Only 100 events per second remain after L3. For the $t\bar{t}$ lepton-plus-jets cross-section analysis, the trigger is based on a high p_T electron or muon candidate. An XFT track with $p_T \geq 8$ GeV/c is required to be matched to a calorimeter energy deposit for an electron candidate or to a stub in the CMUP or CMX muon detectors for a muon candidate.

CHAPTER 3

High Level Object Reconstruction

This chapter presents how high-level objects used in this analysis are reconstructed, namely the charged lepton candidate, missing transverse energy ($\not\!\!E_{\rm T}$) and primary vertex candidates (PVs).

3.1 Charged Lepton

Central electron candidates are reconstructed in the $|\eta| < 1$ region as a central electromagnetic calorimeter energy deposit matched to a COT track. As seen in Fig. 2–5, COT tracking is not reliable in the $|\eta| > 1$ region due to fewer available tracking layers. Plug electron candidates are reconstructed in the $|\eta| > 1$ region as energy deposits in the plug electromagnetic calorimeter only. CMUP (CMX) muon candidates are reconstructed as stubs in the CMU and CMP (CMX) chambers of the muon detection system matched to a COT track. A muon candidate must have an energy deposit in the electromagnetic and hadronic calorimeters consistent with the deposit of a minimum ionizing particle. Muon candidates originating from a cosmic-ray event are vetoed by a cosmic-ray tagging algorithm based on timing information and COT hits [42]. Reconstructing central electrons is more efficient than reconstructing plug electrons or muons. Therefore, we choose the central electron to be our charged lepton in this analysis. In the following paragraphs the central electron event selection is explained in great detail.

In order to reconstruct central electron candidates, first an axial COT track is reconstructed as a series of segments in the axial COT superlayers, which are then fitted to a common circle by two complementary algorithms. The axial COT track is then associated with segments in the stereo superlayers in order to reconstruct a 3D COT track. Central electron candidate COT tracks are required to have at least 3 axial and 2 stereo COT segments, each segment

having at least 5 hits per superlayer. Finding COT tracks with $p_T > 10$ GeV/c in the COT fiducial region is $98.3 \pm 0.12\%$ efficient. This efficiency is measured using $W^{\pm} \rightarrow e^{\pm}\nu$ [42]. A progressive outside-in tracking algorithm also takes into account silicon information and then refits the track in order to improve the track position resolution. Associating at least three silicon hits to an isolated COT track is estimated to be $91 \pm 1\%$ efficient [42].

An electron calorimeter cluster contains a seed tower and at most an additional tower. Then, seed towers are required to contain a transverse energy deposit larger than 2 GeV and to match an extrapolated COT track. Additional towers must lie in the same (adjacent) ϕ (η) wedge as seed towers.

Central electron candidates reconstructed in regions of the CDF detector that are not well instrumented are ignored. Such is the $|z| < 9\ cm$ ($\eta \approx 0$) region where the two half barrels meet. The same goes for the $0.77 < |\eta| < 1.00$ and $75° < \phi < 90°$ region that surrounds the cryogenic connections to the solenoid magnet. Central electron candidates from well instrumented regions are required to pass further selection criteria that are presented in the following paragraphs.

As electron showers are usually contained fully within the electromagnetic part of the calorimeter and hadronic showers spread over both its electromagnetic and hadronic parts, the energy deposit in the electromagnetic calorimeter comes both from electron and hadronic showers. We therefore require central electron candidate clusters to have $E_{had}/E_{em} < 0.055 + 0.00045 \cdot E$, where E_{em} (E_{had}, E)is the electromagnetic (hadronic, total) energy deposit in this cluster measured in GeV.

Very relativistic electrons have a ratio energy over momentum (both measured in GeV) just slightly larger than one ($\frac{E}{p} \succeq 1.0$). If electrons radiate a photon while in the tracking systems, the momentum measurement in the tracking systems accounts only for the momentum of the electron after it radiated the photon, whereas the energy measurement in the calorimeters accounts for the energies of both the electron and the photon. Therefore, the experimental value of the ratio energy over momentum is larger than one ($\frac{E}{p} > 1.0$) but should not be

very large. Hence, central electron candidates are required to have this ratio smaller than two ($\frac{E}{p} < 2.0$). Since this cut is not reliable for large energy deposits, the cut is applied only for central electron candidate clusters with transverse energy deposits smaller than 100 GeV.

The CES detector measures the maximum of the electron shower with the central electromagnetic calorimeter. A variable called L_{shr} compares the lateral shower profile in data and test beam electron data. The lateral shower profile describes the distribution of energies of adjacent central electromagnetic towers as a function of the energy of the seed tower, but also the lateral shower profile within a single tower. Also, a χ^2 comparison is made between CES lateral shower profile from data and the CES lateral shower profile rom electron test beam data. We require central electron candidates to satisfy $L_{shr} < 0.2$ and $\chi^2 < 10.0$. [32].

Furthermore, since energy clusters must be matched to COT tracks before being considered central electron candidates, we can improve our central electron candidate selection by rejecting events based on a track-shower matching variable. We define Δx as the distance between the CES cluster shower and the extrapolated beam constrained COT track in the r-ϕ plane. We multiply this by the charge of the electron/positron candidate in order to account for asymmetric tails due to bremsstrahlung radiation. We then require $-3.0\ cm \leq Q \cdot \Delta x \leq 1.5\ cm$. We define Δz as the distance between the same entities in the r-z plane. There are no asymmetries and we thus require $|\Delta z| \leq 3.0\ cm$.

Next the central electron candidate calorimeter cluster is required to be isolated from clusters from other particles since the charged lepton is a prompt particle emerging directly from the event PV and not from the decay of a long lived particle, such as a bottom quark. Therefore, an isolation variable I is defined as the ratio of energy deposited in the adjacent clusters of the central electron candidate cluster found in a cone of radius $R = \sqrt{(\Delta\phi)^2 + (\Delta\eta)^2} = 0.4$ around the central electron candidate cluster and the energy deposited in the central electron candidate cluster. Central electron candidates are required to have $I \leq 0.1$.

Central electron candidates are vetoed if they originate from a photon conversion, i.e., if another track of opposite electric charge is found with a small distance of closest approach to the central electron candidate's track.

3.2 Missing Transverse Energy

Weakly interacting neutrinos from the W boson decay appear as missing energy because they leave practically no energy deposit in the detector. Beam momenta in the transverse and z directions are known. However, due to the structure of hadrons, colliding partons carry only an unknown fraction of the energy of the protons and antiprotons to which they belong. Therefore, the energy and momenta of the initial state particles are unknown and, even if the energy and momenta of the final state particles are known, energy and momentum conservation cannot be applied. However, due to the small transverse spread of the beam, one does assume both partons to be at rest in the transverse direction and therefore transverse energy and momentum conservation can be applied. The neutrino signature is therefore missing transverse energy ($\not\!\!E_{\mathrm{T}}$). It is to be remarked that this is particular to hadron machines. Energy and momentum conservation can be applied in all directions to electron-positron machines because the charged leptons have no structure and thus the whole energy of the beam goes into collision energy.

Missing transverse energy is defined as the negative of the vector sum of the transverse energy deposited in each calorimeter tower, i.e. $\not\!\!E_{\mathrm{T}} = -\sum_i (E_i \sin\theta)$. One remarks that if our charged lepton is a muon and not an electron, the $\not\!\!E_{\mathrm{T}}$ needs to be corrected in order to take into account the energy the muon leaves in the calorimeter as a minimum ionizing particle. Thus, the muon energy is subtracted from the calorimeter energy deposit and its $\vec{p_T}$ is added to the $\not\!\!E_{\mathrm{T}}$ vector sum.

3.3 Primary Vertex

CDF uses two main algorithms to reconstruct primary vertices (PVs) [43]. The locus of all PVs represents the beamline, or the luminous region of the detector.

The ZVertexFinder algorithm [44] takes as an input a set of tracks passing minimum quality requirements based on the number of silicon and COT hits. The algorithm computes an error weighted average (z_0) of z coordinates of these tracks. z_0 is given by $z_0 = \sum_i (z_i^0/\delta_i^2) \,/\, \sum_i (1/\delta_i^2)$. The algorithm outputs a collection of PVs characterized by their own quality, track multiplicity, z position, z position error and transverse momentum. However, PVs output by the ZVertexFinder algorithm present no x and y position information. Each reconstructed PV corresponds either to hard scattering, or an underlying event of a hard scattering. It may also happen that a physical PV gets reconstructed into two PVs due to tracking resolution. The PV transverse momentum ($p_{T,PV}$) is defined as the sum of the transverse momenta of its tracks ($\sum_{tracks} p_T$) and conveys the information of how energetic a PV is. Typical top-quark PV candidates have ($\sum_{tracks} p_T$) on the order of 100 GeV. The PV quality conveys the information of how well the PVs are reconstructed. PV quality is based on the track multiplicity, as shown in Table 3–1.

Table 3–1: Primary Vertex Quality Criteria

Criterion	Quality Value
Number Si -tracks$\geq$3	1
Number Si -tracks$\geq$6	3
Number COT-tracks$\geq$1	4
Number COT-tracks$\geq$2	12
Number COT-tracks$\geq$4	28
Number COT-tracks$\geq$6	60

The PV with the best chances to be the PV of the interaction triggered on is considered the event PV. The CDF collaboration used to use a run-averaged beamline position as an event PV. CDF developed in 2003 an algorithm called the PrimeVertexFinder [45] that reconstructs a 3D event PV on an event by event basis. This algorithm allowed CDF to improve the efficiency of identifying jets as originating from a bottom quark (b-tagging) for shorter secondary vertex displacements and to reduce the systematic uncertainties due to the run-dependent beam

position variation. PrimeVertexFinder takes as an input a set of good quality tracks in good agreement ($\chi^2 < 10$) with a seed vertex (usually the beamline position or one of the PVs output by ZVertexFinder). These tracks are reconstructed to a new 3D PV and checked if they are still in good agreement with the new PV. Tracks with $\chi^2 > 10$ are rejected. The remaining tracks are reconstructed to a new 3D PV. The procedure is iterated until all remaining tracks have a $\chi^2 < 10$ with respect to the latest PV. The last 3D PV becomes the event PV. 3D position information is crucial for b-tagging techniques that use the information about the bottom quark lifetime.

A PV typical position is represented by (x_{PV}, y_{PV}, z_{PV}). A typical longitudinal width is $\sigma_z = 29\ cm$. A typical transverse width is circular, smaller at the center of the detector, $\sigma_{\perp,z=0\ cm} = 30\ \mu m$ and larger at extremities, $\sigma_{\perp,z=40\ cm} \simeq 50\ \mu m$. Typical x_{PV} and y_{PV} are very small, on the order of tens of microns. Event PV reconstruction is trusted only in the luminous region ($|z_{PV}| \leq 60$ cm). Events with the event PV outside the luminous region are rejected (luminous cut).

CHAPTER 4
Event Selection

4.1 Lepton plus Jets

A typical top-quark pair event selection in the lepton-plus-jets channel selects events with one and only one high-p_T charged lepton (e or μ), large missing transverse energy ($\not\!\!E_{\rm T}$) and four high-p_T jets (two of which can be b-tagged).

The lepton-plus-jets sample doesn't contain only $t\bar{t}$ events. Table 4–1 presents the cross-sections of the expected signal and background for the lepton-plus-jets channel [46] [?, ?]. The largest source of background is represented by the production of a W boson and quarks (W+jets). Other sources of background exist, but are much smaller. For instance, there are: the diboson electroweak production, when one boson decays leptonically and the other hadronically; the production of a Z boson that decays to a $\tau\bar{\tau}$ lepton pair; the $q\bar{q}$ annihilation in the W^* (s-channel) resulting in single top produced in association with a bottom quark; the W boson-gluon fusion in the t channel where a gluon splits to a $b\bar{b}$ pair and where the virtual W boson interacts with a b quark.

Once the events are selected, a series of cuts is applied in order to maximize the signal over background ratio. Electrons or positrons must not come from conversions of photons into electron-positron pairs (conversion veto). Muons must not come from cosmic rays (cosmic ray veto). Two-lepton events that are used for analysis in the dilepton channel, where both W bosons decay leptonically, are explicitly removed (dilepton veto), so that the lepton plus jets samples and the dilepton samples are orthogonal. This makes it easier to combine results from these two channels. Events with a charged tight lepton and another object forming an invariant mass within the Z mass window ([76,106] GeV/c^2) are removed (Z boson veto). One

Table 4–1: Lepton-plus-jets signal and background cross section values

Element	Type	Cross section (pb)
$t\bar{t}$	Signal	7.3
W+0 jets	Background	1790
W+1 jets	Background	225
W+2 jets	Background	35.5
W+3 jets	Background	5.63
W+4 jets	Background	1.50
WW	Background	13.25
WZ	Background	3.96
ZZ	Background	1.58
$Z \rightarrow \tau^+\tau^-$	Background	254.3
Single top W^* (s-channel)	Background	0.88
Single top W-g (t-channel)	Background	1.98

way of b-tagging a jet is by observing that the secondary vertex produced by the decay of the bottom quark is displaced from the 3D event PV (SecVtx algorithm). As shown in the previous chapter, the 3D event PV is reconstructed by the PrimeVertexFinder algorithm, which inputs the z position of one of the PVs in the event as a seed. Tagging efficiently a bottom quark jet requires reconstructing correctly the 3D event PV, which requires choosing correctly the (1D) event PV. Furthermore, a series of cuts is applied based directly on the z position of the (1D) event PV. The (1D) event PV will be studied in this dissertation.

PV quality is defined as the sum of the quality values of tracks that are used to reconstruct the PV. From the many PV in the event output by the ZVertexFinder algorithm, we consider in this study only the PVs with a quality larger than 12 (Table 3–1). Good quality PVs typically contain two good quality COT tracks. One of the remaining PVs is selected to be the (1D) event PV. If no good quality PV is reconstructed in the event, the event PV z position is considered the z position of the charged lepton. A cut is applied on the z position of the chosen PV. Thus, only events with PV z position in the luminous region are accepted ($z_{PV} \leq 60$ cm). Another cut is applied on the z distance between the chosen PV and the charged lepton. Currently at CDF, events are rejected if this distance is larger than 5 cm. This cut is needed in order to

ensure that the high-p_T charged lepton is coming from the event PV. The promptness of the $t\bar{t}$ pair decay (section 1.2.3) means that the charged lepton originates from the primary vertex. Because of the detector resolution, however, the charged lepton and the PV would have close but not identical z positions.

4.2 Primary Vertex Study

As we have seen in section 4.1, the (1D) event PV plays an important role in the top-quark pair event selection in the lepton-plus-jets channel. One should remark that it is also important in all channels of top-quark analysis, but also in other analyses that involve prompt charged leptons, jets or secondary vertices (identifying jets originating from bottom and charm quarks and from the tau lepton). In this dissertation we perform a systematic study of the (1D) event PV in the lepton-plus-jets channel. The conclusions we obtain are to be used only in this context. This study could easily be extended to be used for various CDF analyses, as described above.

For the study performed in this analysis, we select events with one and only one very energetic central electron ($p_T \geq 20\text{GeV}/c$), large missing transverse energy ($\not\!\!E_T \geq 20\text{GeV}/c$) and at least one good quality PV. Within one event that passes our selection criteria, we consider only good quality PVs in the luminous region. Since central electrons are reconstructed more efficiently than plug electrons or muons, the charged lepton of this analysis is considered the central electron.

CHAPTER 5

Primary Vertex Study

A typical event may have more than one reconstructed PV for various reasons. First, consider a $p\bar{p}$ bunch crossing with only one hard parton-parton scattering. Although the remnant partons from the hadrons participating in this scattering usually continue down the beam pipe, it may happen that these remnants are scattered into the detector and form PVs of their own. Their energy deposit in the detector is called the underlying event. The underlying event at CDF is described in detail in Ref. [48]. The energy deposits of the underlying event overlap with the energy deposits of the $t\bar{t}$ interactions. Therefore, energy measurements have to be corrected for the underlying event. Second, there are often more than one hard parton-parton scattering per bunch crossing due to large instantaneous luminosities. Each hard parton-parton scattering creates its own PV, one of which may create a $t\bar{t}$ pair. The PV associated with the $t\bar{t}$ pair is defined to be the "true" event PV. Various detector algorithms select one or another PV as the event PV. Third, it may happen that a true physical PV is reconstructed into two or more PVs due to limited tracking resolution. In this case two PVs close in the z coordinate may exist. On the other hand, it may happen that a true physical PV does not get reconstructed at all if some of the tracks lie outside the luminous region of the detector or if they leave very few silicon and COT hits. Also, the whole PV is ignored if it is situated outside of the luminous region. In conclusion, there may be more than one PV per event. The physical primary vertex is a point in 3-dimensional space (3D PV). However, since the transverse position is very close to the beamline, it is mostly the z position of the primary vertex that matters for this analysis. A primary vertex characterized only by its z position is a 1D PV. 1D PVs are reconstructed

by the ZVertexFinder algorithm. One of these 1D PVs must be chosen as the event PV. In the following, by "PV" we mean "1D PV".

Current Tevatron instantaneous luminosities on the order of $50 \cdot 10^{30} cm^{-2} s^{-1}$ produce an average of 1-2 PVs/event. However, the Tevatron is continuously increasing its average instantaneous luminosity and, by 2009, when the Tevatron is expected to shut down, there is expected to be on average 4-5 PVs/event at an average instantaneous luminosity of $300 \cdot 10^{30} cm^{-2} s^{-1}$. Choosing the correct event PV is essential in order to be able to perform many analyses. Choosing the event PV becomes harder at higher instantaneous luminosity regimes. Therefore, it is important to develop and validate algorithms and techniques now, so that these may be used later, both at the Tevatron and the LHC. In the first years after startup, the LHC will run in a low luminosity regime of $1,000 \cdot 10^{30} cm^{-2} s^{-1}$ and produce 2-3 PVs/event, about the same PV multiplicity CDF and DZero currently encounter at the Tevatron. Afterwards, the LHC will upgrade to its design luminosity and there will be on average 25 PVs/event at $10,000 \cdot 10^{30} cm^{-2} s^{-1}$. Table 5–1 summarizes the average PV multiplicity as a function of the instantaneous luminosity at the Tevatron and LHC accelerators.

Table 5–1: Average PV multiplicity as a function of instantaneous luminosity at the Tevatron and LHC accelerators

Accelerator	Instantaneous Luminosity	Number of PVs/event
Tevatron now RUN II	$50 \cdot 10^{30} cm^{-2} s^{-1}$	1-2 PVs
Tevatron end RUN II	$300 \cdot 10^{30} cm^{-2} s^{-1}$	4-5 PVs
LHC first years	$1,000 \cdot 10^{30} cm^{-2} s^{-1}$	2-3 PVs
LHC nominal	$10,000 \cdot 10^{30} cm^{-2} s^{-1}$	20-25 PVs

5.1 Motivation

As presented in the previous section, our goal is to choose the correct $t\bar{t}$ PV candidate from a collection of PVs on an event by event basis. This is essential for many analyses. In

this dissertation we perform the PV study in the context of top-quark pair analyses in the lepton-plus-jets channel. This study is important for several reasons.

First, in the lepton plus jets event selection, cuts are applied directly on the event PV z position. A first cut accepts only event PVs inside the luminous region of the detector ($|z_{PV}| \leq 60$ cm). The 60 cm value is well motivated, as it represents 2 sigma of the longitudinal z beamline position. The charged lepton is prompt and emerges from the event PV. However, due to tracking resolution, the z position of the charged lepton may not be identical to that of the event PV. This is why CDF currently uses a second cut to accept only events for which the charged lepton is not further away than 5 cm from the chosen event PV in the z coordinate. However, the 5 cm value is not well motivated and seems a priori arbitrary. To confirm that it is the right value to use, or to propose a new value, we perform Monte Carlo studies.

Second, the z position of the $t\bar{t}$ PV candidate is used to cluster jets. This is why the error on the jet energy (jet energy scale) can be decreased if the z position of the $t\bar{t}$ event PV candidate is correctly measured. Although studies at CDF have shown that this effect is small, since a 5% error in the jet energy scale being expected for a 10 cm error in the measurement of the position of the event PV [49], decreasing the jet energy scale is essential in decreasing the uncertainty on the top-quark mass. .

Third, the z position of the (1D) PV is input as a seed in the PrimeVertexFinder algorithm that outputs a (3D) event PV used in tagging of jets possessing a displaced secondary vertex with respect to this primary vertex. 3D information is needed to compute the transverse (xy) distance between the secondary vertex and the primary vertex. Therefore, identifying the correct (1D) PV improves b-tagging, which is important to enrich the signal over background ratio in $t\bar{t}$ samples.

Fourth, a CDF analysis measures directly the top-lifetime by measuring the distance from the $t\bar{t}$ reconstructed PV to the projection in the r-ϕ plane of the electron track. A public note of this analysis is presented in Ref. [50].

5.2 Event PV Algorithms

The previous section presented reasons for the importance of picking correctly on an event by event basis the $t\bar{t}$ PV candidate from a collection of PVs offered by the ZVertexFinder algorithm. There are possible ways to choose the $t\bar{t}$ PV candidate. The successful candidate should be both very energetic and very close in the z direction to the charged lepton. The event PV should be very energetic since the $t\bar{t}$ pair is very massive. At the same time, the event PV should be very close in z to the charged lepton since the latter is prompt and emerges from the event PV, but due to tracking resolution it has a close, but not identical, z coordinate to the event PV.

Therefore, two major algorithms that select the $t\bar{t}$ PV candidate appear naturally. The first one picks the most energetic PV in the event. The second one picks the PV that is the closest in the z coordinate to the charged lepton. This latter definition is currently used by the CDF Collaboration [51].

5.3 Analysis Method

For each event there is a central electron and a collection of reconstructed primary vertices (PVs). For a Monte Carlo (MC) event there is also a true primary vertex read from the MC truth information. Only for MC events we can thus check if the event PV chosen by a particular algorithm was chosen correctly. We can therefore compute an efficiency of the event PV selection. We can then evaluate the efficiency of the event PV-charged lepton distance cut as a function of the distance cut value. Next, we can evaluate the $t\bar{t}$ signal over the W+jets background significance as a function of the cut value. The event PV selecting algorithm that maximizes event PV efficiency is preferable. The distance cut value that maximizes the signal over background significance is the optimal cut value.

5.4 High Luminosity Regime

We first look at a $t\bar{t}$ signal Monte Carlo sample with minimum bias events overlaid at a high luminosity regime. This MC sample contains six runs and on the order of 29,000 events.

Run averaged instantaneous luminosities span the interval $50 \cdot 10^{30} cm^{-2} s^{-1}$ (the current average instantaneous luminosity at CDF) to $300 \cdot 10^{30} cm^{-2} s^{-1}$ (the estimated instantaneous luminosity in 2009, when CDF is expected to stop taking data). The instantaneous luminosity step between each run is $50 \cdot 10^{30} cm^{-2} s^{-1}$. This Monte Carlo sample uses Pythia [52] as the event generator, QQ [53] as the decay generator, a GEANT3-based [54] detector simulation package and an assumed top-quark mass of 175 GeV/c^2. The CDF Monte Carlo machinery proved to be robust in describing the collision interactions and particle interactions with the detector material [42]. The accuracy is improved by overlaying minimum bias events with multiplicities consistent with expectations at a given instantaneous luminosity. More information on the simulation of the CDF detector can be found in Ref [55]. The primary vertex multiplicity distribution is given by a Poisson random based distribution measured in data. The MC samples reconstruct slightly less PVs than the data samples, but the difference is very small and can be neglected. From this MC sample, 28,392 events pass the event selection criteria and are studied in the following paragraphs. Their normalized PV multiplicity distribution is presented in Fig. 5–1. The distribution peaks at 2 PVs/event and has a mean of 2.89 ± 0.02. We remark that there are events with up to 9 PVs.

For every event there is a charged lepton (Lep) and a collection of reconstructed primary vertices (PVs). The variable $\sum_{tracks} p_T$ measures how energetic a reconstructed PV is. The first algorithm chooses as event PV the most energetic reconstructed PV (PV_1). The second algorithm chooses as event PV the reconstructed PV closest in z to the charged lepton (here the central electron)(PV_2). Furthermore, we can know what is the true PV ($TruePV$) using the Monte Carlo truth information. The $TruePV$ is also reconstructed and has a different z position than any of the reconstructed PVs, but is very close in z to one of the PVs. We consider the reconstructed PV that is the closest in z to the $TruePV$ to be the correct event PV ($CorrectPV$). We are confident in this matching thanks to very close $TruePV$ and $CorrectPV$ z positions (Fig. 5–2).

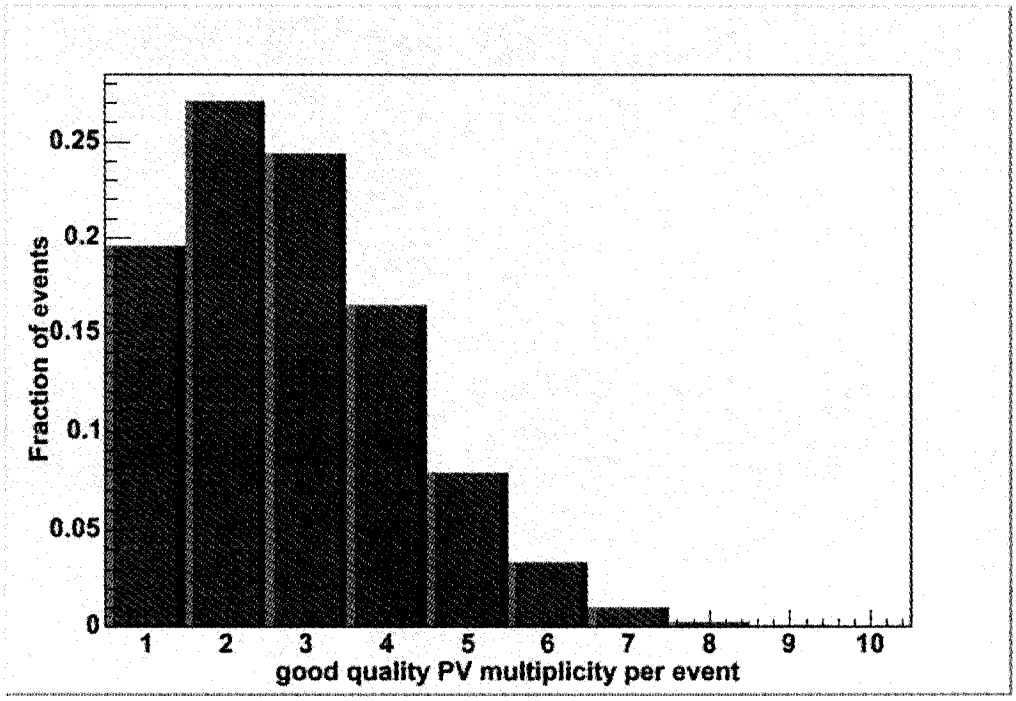

Figure 5–1: Normalized distribution of number of PVs/event in the high luminosity MC sample for all runs combined.

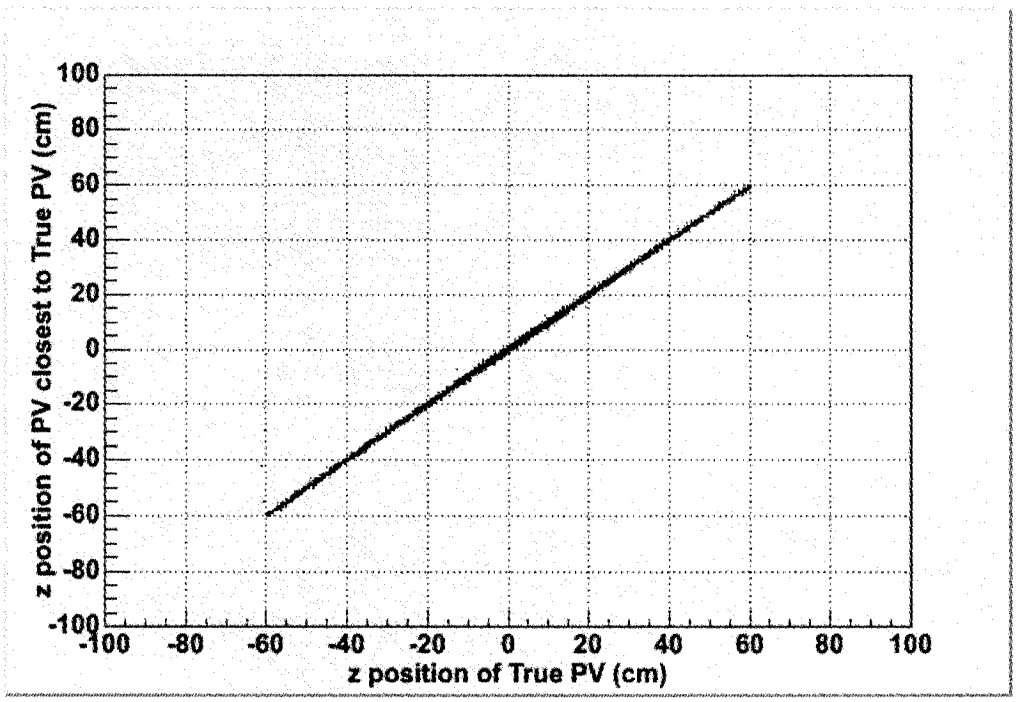

Figure 5–2: Z position of $TruePV$ (x axis) versus z position of the reconstructed PV closest in z to $TruePV$ ($CorrectPV$) (y axis)

Fig. 5–3 presents the z position of PV_1, PV_2, Lep and $CorrectPV$. We observe that these distributions are almost identical, which means that in most cases the reconstructed PVs are very close to the $TruePV$ and to the charged lepton, as expected. However, they are not identical and Fig. 5–4 presents the ratios of the z positions of the PV_1, PV_2 and Lep with respect to the $CorrectPV$ z position. There is very good agreement between all these variables in the central detector region and differences appear at the extremities of the luminous regions, where the tracking gets worse, again as expected.

As we compare the values of z positions of these four variables, we also need to understand their z position uncertainties. These errors are plotted in Fig. 5–5 on logarithmic vertical and horizontal scales. Primary vertices used in this analysis are good quality tracks (quality larger than 12) and are formed by at least two tracks. Typical such PV z position uncertainties are on the order of 100 μm. A typical track z position uncertainty is 70 μm. A PV formed by N tracks has a z position error given by the formula $e_{PV} = \frac{\sqrt{\sum_{track=i}^{track=N} e_{track}}}{N}$. Typical central electron position errors are larger. The lepton position error is about 100 μm if all silicon hit information is used, 1 to 3 mm if only small-angle stereo silicon information is used and 5 mm if no silicon information is used. Since the central electron z position error is at least one order of magnitude larger than the z position on the PVs, a significance study of the overlap of one PV and the central electron is not sensitive. We tested this type of study and found it inconclusive, as expected.

A total of 28,392 events pass the event selection criteria. We want to know for how many of these events does algorithm 1 (2) pick correctly the event PV. In other words, we want to estimate the efficiency of correct event PV identification for each algorithm. Fig. 5–6 offers a qualitative approach of the event PV selection for both algorithms for all events, for events with a PV multiplicity of 2 and for events with a PV multiplicity of 5. In this figure, bin 1 represents the fraction of events for which algorithm 1-selected event PV is the same as the correct event PV as read from the MC truth information and bin 2 presents the fraction of

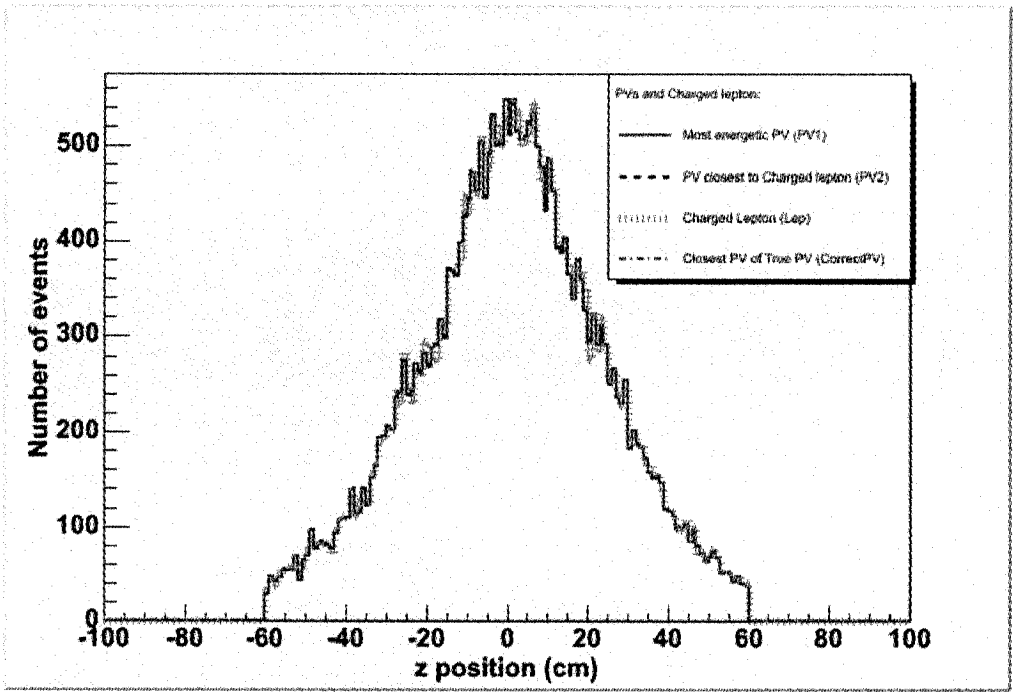

Figure 5–3: Z position distribution of PV_1, PV_2, Lep and $CorrectPV$

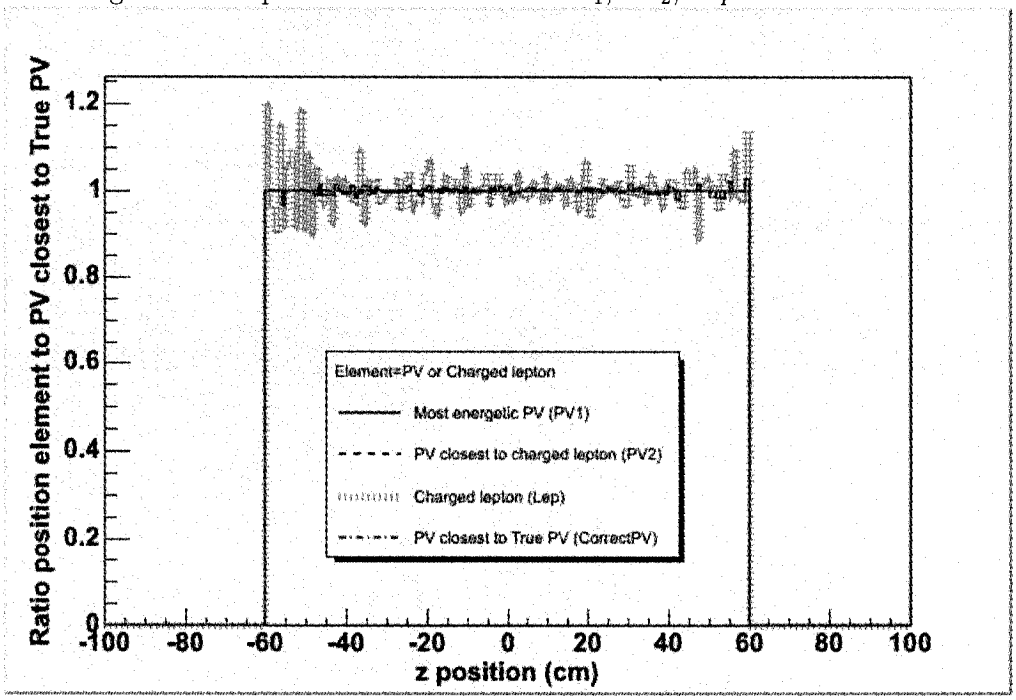

Figure 5–4: Ratios of z positions of PV_1, PV_2, Lep and $CorrectPV$ to the z position of $CorrectPV$.

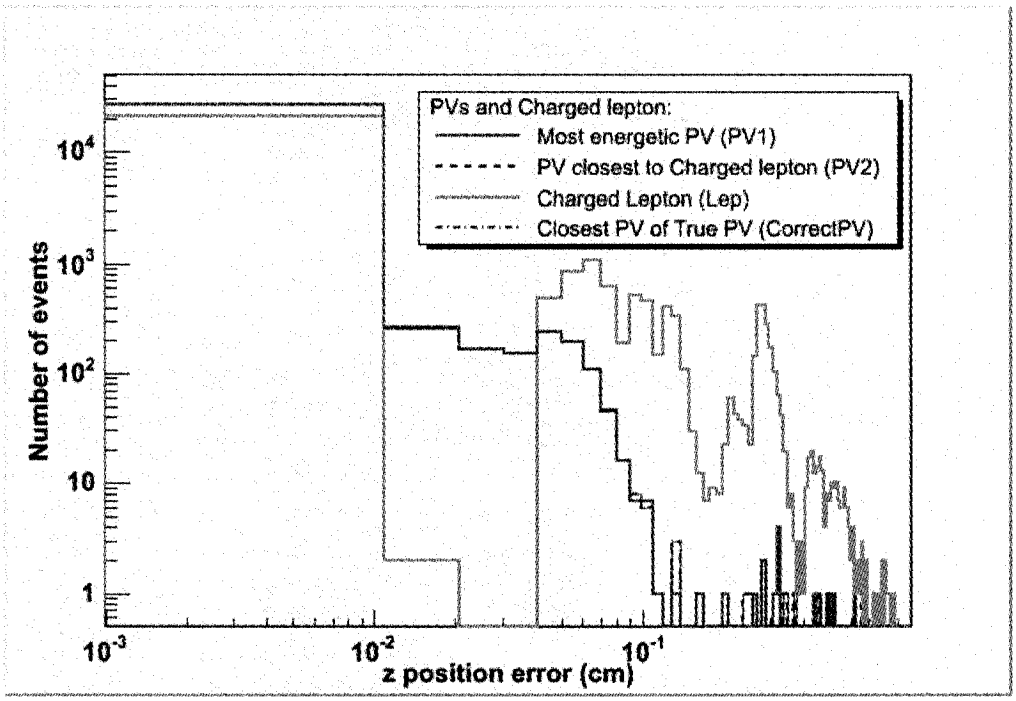

Figure 5–5: Z position error distribution of PV_1, PV_2, Lep and $CorrectPV$

events for which this does not happen. The sum of the fractions in bins 1 and 2 is unity. Bin 3 and 4 present the same thing for algorithm 2. Bin 5 presents the fraction of events for which both algorithms select the correct event PV. Bin 6 presents the fraction of events for which both algorithms select incorrectly the event PV. Bin 7 presents the fraction of event for which algorithm 1 selects correctly the event PV but algorithm 2 selects incorrectly the event PV. Bin 8 presents the fraction of event for which algorithm 1 selects incorrectly the event PV but algorithm 2 selects correctly the event PV. Bin 9 presents the fraction of event for which both algorithm select the same event PV, but not necessarily the correct one. Bin 10 presents the fraction of events for which the two algorithms select different event PV and therefore at least one of them selects the wrong event PV. Table 5–2 presents a quantitative approach for the same situation for the high luminosity $t\bar{t}$ signal MC sample.

Table 5–2: Quantitative aspects of event PV selection efficiency for each algorithm in the high luminosity minimum bias event $t\bar{t}$ signal MC data sample. The table presents number of events, efficiency for both algorithms to select correctly the event PV, probability that both algorithms select the same PVs. Errors are binomial and statistical only.

No PVs	No. Evts.	Eff. PV_1	Eff. PV_2	Prob PV_1 same PV_2
all	28,392	0.9975 ± 0.0003	0.9994 ± 0.0002	0.9972 ± 0.0004
1 PV	5286	1 ± 0	1 ± 0	1 ± 0
2 PVs	7465	0.9985 ± 0.0005	0.9995 ± 0.0003	0.9985 ± 0.0005
3 PVs	6901	0.9984 ± 0.0005	0.9990 ± 0.0004	0.9977 ± 0.0006
4 PVs	4822	0.9960 ± 0.0010	0.9992 ± 0.0005	0.9960 ± 0.0010
5 PVs	2416	0.995 ± 0.002	0.999 ± 0.001	0.994 ± 0.002
6 PVs	1048	0.995 ± 0.003	0.999 ± 0.001	0.994 ± 0.003
7 PVs	328	0.991 ± 0.005	1 ± 0	0.991 ± 0.005
8 PVs	100	0.99 ± 0.01	0.99 ± 0.01	0.99 ± 0.01
9 PVs	23	0.96 ± 0.04	1 ± 0	0.96 ± 0.04

We deduce that algorithm 2 is more efficient than algorithm 1 in selecting the correct event PV, namely that the closest PV to the charged lepton is more often the correct event PV than the most energetic PV in the event. This happens for all PV multiplicities. Therefore we confirm that CDF is doing the right thing by using currently the algorithm 2 and we recommend

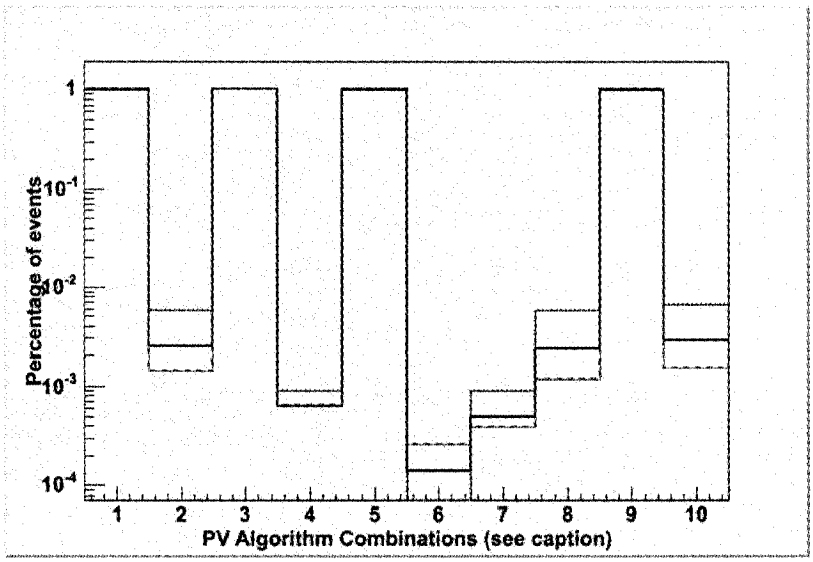

Figure 5–6: Qualitative aspects of event PV selection efficiency for each algorithm in the high luminosity minimum bias event $t\bar{t}$ signal MC data sample for all PV multiplicities (black solid line), PV multiplicity of 2 (red dashed line) and PV multiplicity of 5 (blue dotted line). The various bins represent the percentage of events for various PV multiplicities: Bin 1-PV_1 is $TruePV$; Bin 2-PV_1 is not $TruePV$; Bin 3-PV_2 is $TruePV$; Bin 4-PV_2 is not $TruePV$; Bin 5-Both PV_1 and PV_2 are $TruePV$; Bin 6-Neither PV_1 nor PV_2 are $TruePV$; Bin 7-PV_1 is but PV_2 is not $TruePV$; Bin 8-PV_1 is not but PV_2 is $TruePV$; Bin 9-PV_1 is PV_2; Bin 10-PV_1 is not PV_2

that this algorithm continue to be used as instantaneous luminosity increases. Both efficiencies are nevertheless acceptable, with values very close to 100%. In 28,312 (80) events the two algorithms choose the same (different) event PV. This is consistent with the two algorithms having very close efficiency values. Even if small, we want to understand where these differences come from and see how they change with increasing PV multiplicities (therefore increase in instantaneous luminosity).

Fig. 5–7 presents a rz Event Display zoomed-in view of a MC event from this MC sample for which the most energetic PV (PV_1: $z \approx 6$ cm and $\sum_{tracks} p_T \approx 800$ GeV) is not the event PV, but rather the closest PV to the charged lepton in the z direction (PV_2: $z \approx 42$ cm and $\sum_{tracks} p_T \approx 200$ GeV). For comparison, Fig. 5–8 presents a rz Event Display zoomed-in view of a typical MC event from this MC sample for which each algorithm chooses the same event PV since there is only one PV in the event.

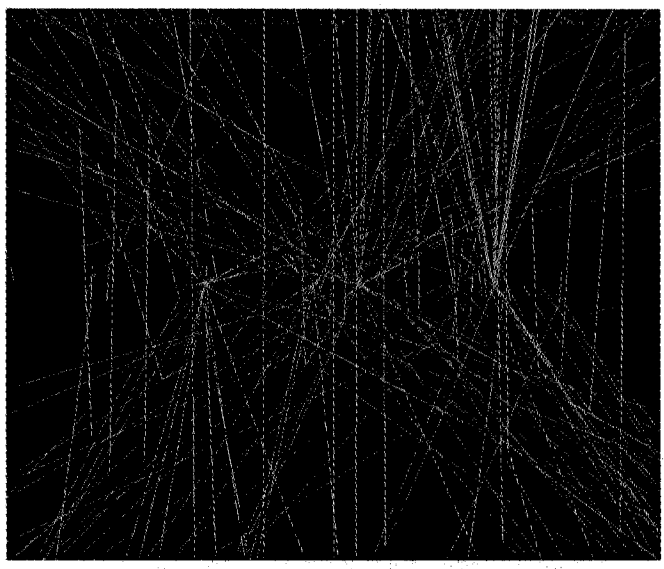

Figure 5–7: rz Event Display view of a MC event for which the most energetic PV (PV_1: $z \approx 6$ cm and $\sum_{tracks} p_T \approx 800$ GeV) is not the event PV, but rather the closest PV to the charged lepton in the z direction (PV_2: $z \approx 42$ cm and $\sum_{tracks} p_T \approx 200$ GeV)

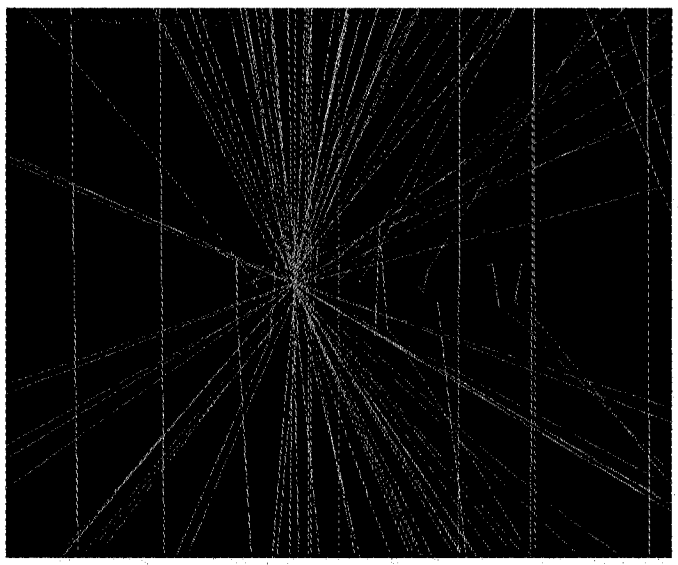

Figure 5–8: rz Event Display zoomed-in view of a typical MC event from this MC sample for which each algorithm chooses the same event PV since there is only one PV in the event

Fig. 5–9 presents the $\sum_{tracks} p_T$ distributions for PV_1 and PV_2 and $CorrectPV$. These distributions are very similar and have the same mean of 174 ± 1 GeV. However, they are not identical. Fig. 5–10 presents the ratios of the $\sum_{tracks} p_T$ of PV_1 and PV_2 to $CorrectPV$. We see big discrepancies for both extremities of the $\sum_{tracks} p_T$ distributions.

Fig. 5–11 presents the distributions of the z distance between the PVs selected by each algorithm and the charged lepton. Clear differences between the two distributions appear at distances larger than 3 cm. As expected, the most energetic PV (PV_1) tends to be further away from the charged lepton than the closest PV to the charged lepton (PV_2).

Since we are looking at distributions of events from a $t\bar{t}$ signal Monte Carlo sample, one PV from each event is a $t\bar{t}$ event PV. The percentage of events for which algorithm 1 (2) chooses correctly the event PV represents the event PV selection efficiency for $t\bar{t}$ signal events for algorithm 1 (2). These efficiencies are presented for events with PV multiplicities of 2 and 5 (Fig. 5–6). For each algorithm, events for which the event PV is not chosen correctly are rejected. Remaining events are then rejected if the event PV charged lepton z distance is larger

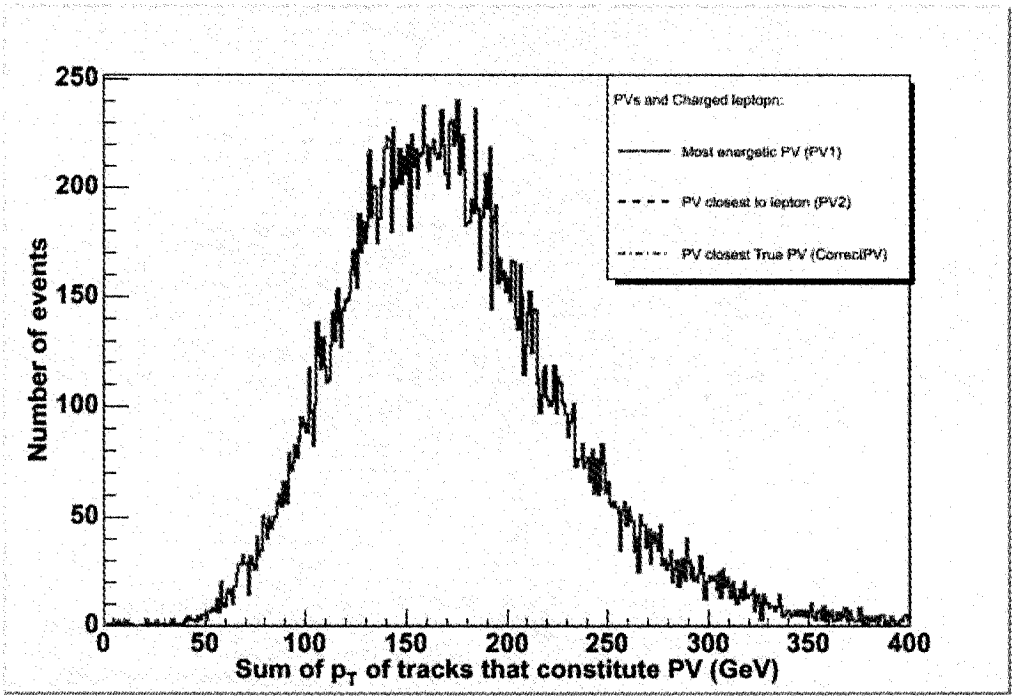

Figure 5–9: $\sum_{tracks} p_T$ distribution for PV_1 and PV_2 and $CorrectPV$

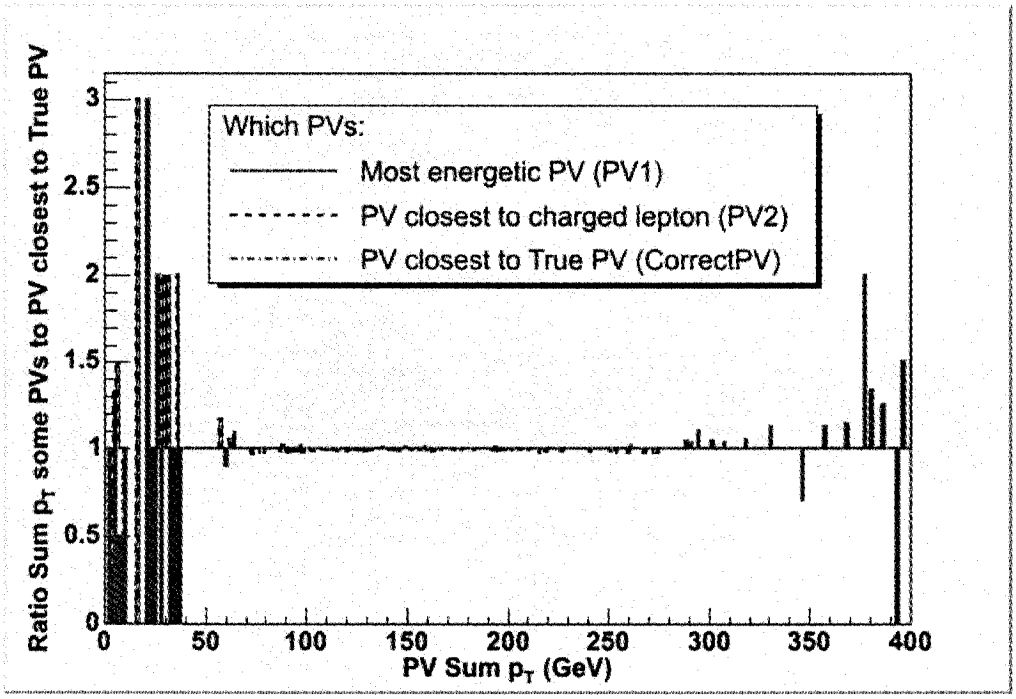

Figure 5–10: Ratios of $\sum_{tracks} p_T$ for PV_1 and PV_2 to $CorrectPV$

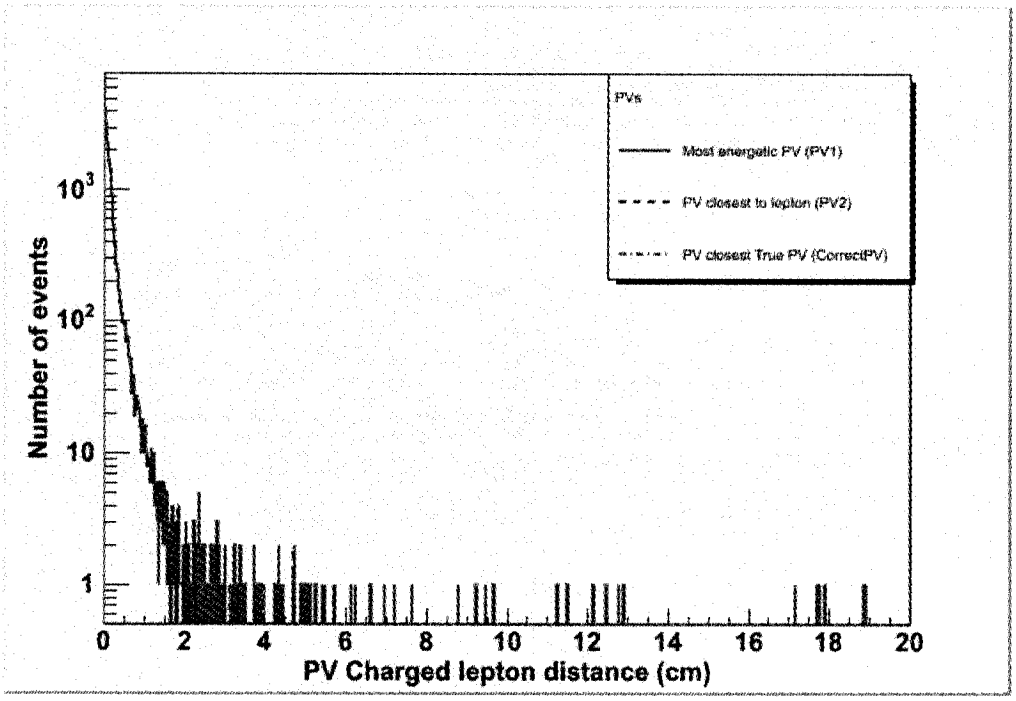

Figure 5–11: Z distance to charged lepton distribution for PV_1 and PV_2

than a certain distance, which is currently 5 cm. The percentage of events that remain following this cut after the event PV was chosen using algorithm 1 (2) represents the efficiency of the event PV charged lepton z distance cut in the case algorithm 1 (2) is used to identify the correct event PV. These efficiencies are presented for events with PV multiplicities of 2 (Fig. 5–12) and 5 (Fig. 5–13) on zero suppressed plots. Since the We conclude that the algorithm 2 is again more efficient for the event PV-charged lepton distance cut for all values of PV multiplicity.

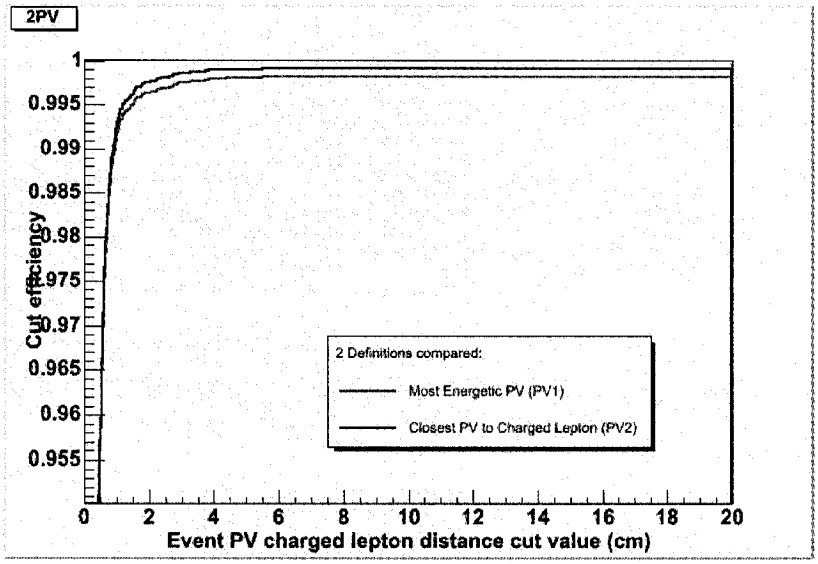

Figure 5–12: Event PV charged lepton z distance cut efficiencies as a function of the cut value, for both algorithms, for events that have 2 PVs on a zero suppressed plot.

5.4.1 Signal over Background Significance

Until now we have studied the signal efficiency for both the event PV selection and the event PV charged lepton z distance cut on a high luminosity MC sample. We then performed a signal over background significance study over MC samples used by the top group in the context of 1 fb^{-1} analyses. The W+i jets and $t\bar{t}$ MC samples used in this part of the study use PYTHIA 6.2. [52], HERWIG 6.510 [56] as event generators, EvtGen [57] as package for b quark decays and GEANT3 [54] as detector simulation package. These MC samples also model minimum bias interactions. We considered the backgrounds of W+i jets, where i varies from 0

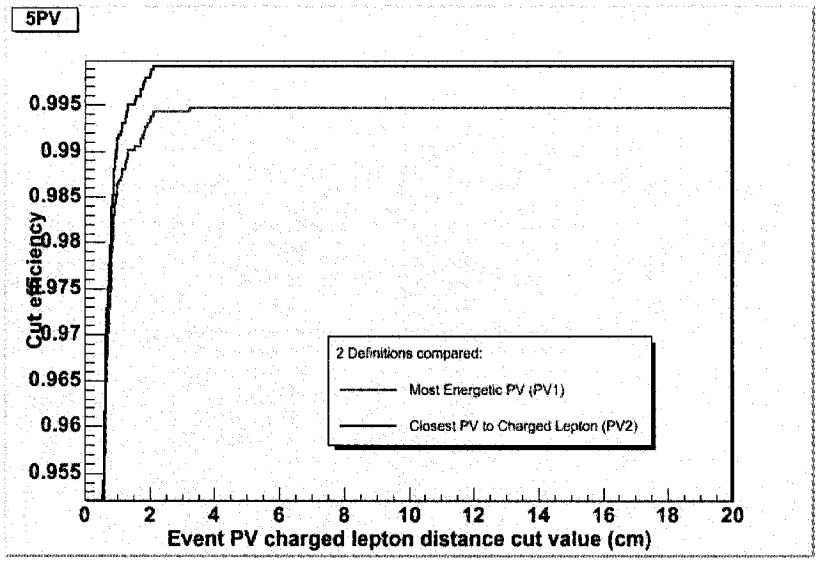

Figure 5–13: Event PV charged lepton z distance cut efficiencies as a function of the cut value, for both algorithms, for events that have 5 PVs on a zero suppressed plot.

to 4. We weighted both signal and background with the appropriate cross section values [46] (Table 5–3).

Table 5–3: Signal and background cross section values

Element	Type	Cross section (pb)
$t\bar{t}$	Signal	7.3
W+0 jets	Background	1790
W+1 jets	Background	225
W+2 jets	Background	35.5
W+3 jets	Background	5.63
W+4 jets	Background	1.50

We plotted the square of the signal over background significance for PV multiplicity values of 2 (Fig. 5–14) and 5 (Fig. 5–15) as a function of the event PV charged lepton distance cut value. Since the signal events are far less numerous than the background events, we use a significance formula of the type $Sig = \frac{S}{\sqrt{S+B}}$. We consider the W+jets backgrounds only, for different numbers i of jets, where both signal and background are weighted by their production

cross sections. We use therefore the formula $Sig = (\sigma_S S) / \left(\sqrt{\sigma_S S + \sum_{i=0}^{i=4} \sigma_{B_i} B_i} \right)$, where σ represents the cross section and S (B_i) represents the number of signal (W+i jets background) events selected. Peaks in these distributions can suggest which event PV charged lepton distance cut value to use for each algorithm. However, we obtained that these distributions are flat for cut values larger than 1 cm for all PV multiplicities. We present here these plots for PV multiplicities of 2 and 5. We conclude that we lack sensitivity and any cut above 1 cm is appropriate. Further studies are needed in order to clarify this issue.

5.4.2 Other Possible Algorithms

Choosing the event PV as either the most energetic PV (algorithm 1) or the PV closest in z to the charged lepton (algorithm 2) comes naturally as the event PV is expected to be both every energetic and very close in z in the charged lepton. Both algorithms choose the same PV as the event PV in most of the cases, which is acceptable for $t\bar{t}$ analyses in the lepton-plus-jets channel. Since this study may be extended to other types of analyses, it is important to analyze some general criteria of better selecting the PVs on which we apply the event PV selection in the first place. For events for which the most energetic and the next to most energetic PV have very different $\sum_{tracks} p_T$ values, the most energetic PV is more likely to be trusted to be the event PV. On the other hand, for events for which these values are very close it is hard to decide which PV to trust to be the event PV. In such cases the z distance between the respective PVs has to be taken into account. In the same idea, events for which one PV is close to the charged lepton in z but the second closest is far away from the charged lepton, we trust the closest PV to be the event PV. On the other hand, if these two PVs are about at the same distance to the charged lepton, it is hard to choose which of the two has a better chance to be the event PV. These arguments suggest that maybe new algorithms for choosing the event PV may be developed. For instance, we could ignore all PVs further away than a certain distance

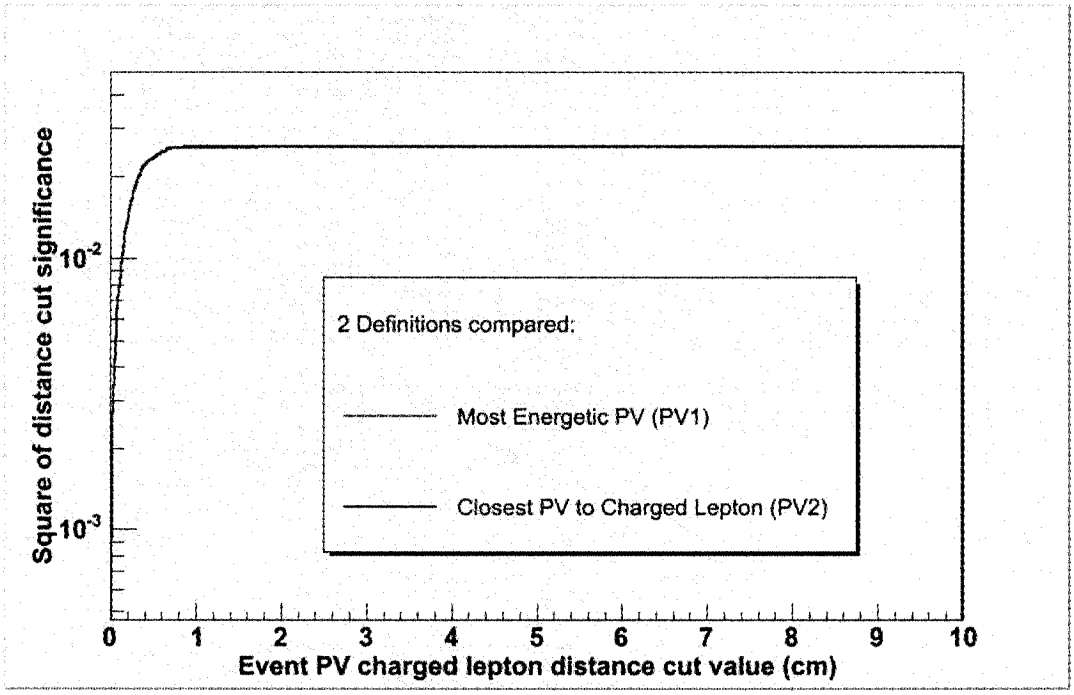

Figure 5–14: Square of signal over background significance for events with a PV multiplicity of 2

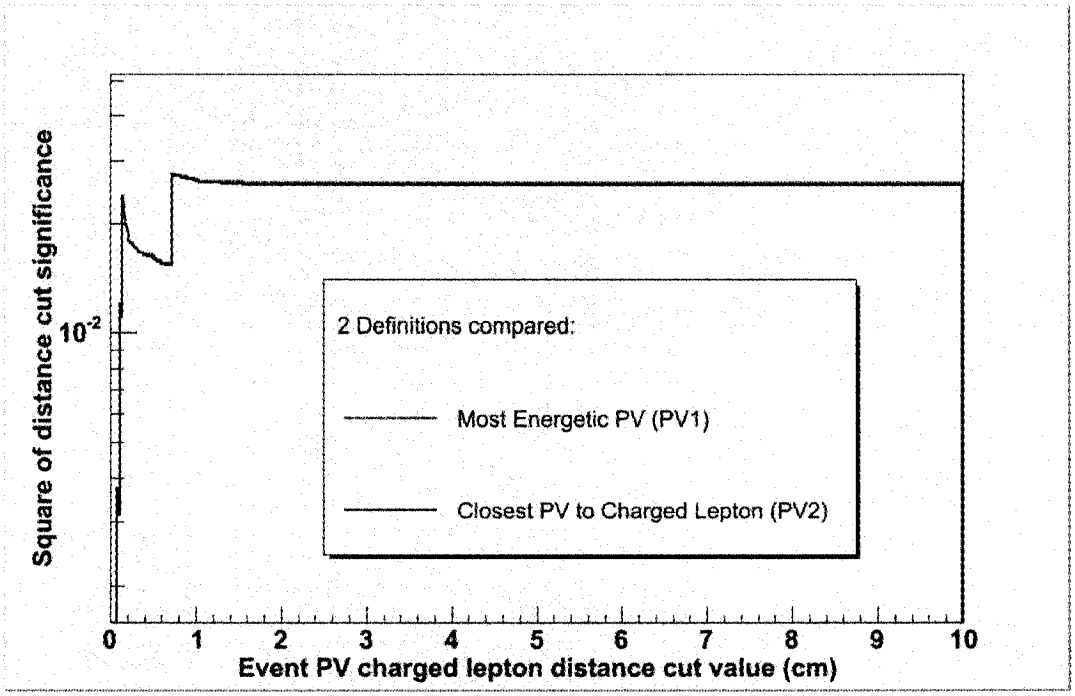

Figure 5–15: Square of signal over background significance for events with a PV multiplicity of 5

around the charged lepton and then consider as event PV the most energetic remaining PV. The efficiency of event PV selection of this algorithm would be a function of this distance.

Also, studying events that do not pick correctly the event PV shows that there are events with very large unrealistic $\sum_{tracks} p_T$ values (more than 1000 GeV/c). When a track is misreconstructed to an almost straight line, the algorithm believes it is a very energetic track. Such tracks may be reconstructed to a PV. However, this track and therefore this PV are not to be trusted. Given that a maximum center-of-mass energy of 1.96 TeV is available for a hard scattering, that colliding partons contain only a fraction of the momentum of the colliding protons and antiprotons, considering only PVs with $\sum_{tracks} p_T$ smaller than a certain value (possibly 1000 GeV/c is a good value) and then choosing the event PV as the most energetic remaining PV is another potential algorithm. The efficiency of event PV selection of this algorithm would be a function of this $\sum_{tracks} p_T$ cut value. Fig. 5–16 presents a rz Event Display view of a MC event where one track is badly reconstructed as an almost straight line and therefore is included in a PV with an unrealistically large $\sum_{tracks} p_T$ (PV_1: $z \approx 6$ cm and $\sum_{tracks} p_T \approx 55,000$ GeV). For this MC event, the event PV is the PV closest in the z direction to the charged lepton (PV_2: $z \approx 31$ cm and $\sum_{tracks} p_T \approx 260$ GeV).

Finally, Fig. 5–17 presents a 2D distribution for events having at least 2PVs per event. The x axis represents the ratio between the next to largest and largest $\sum_{tracks} p_T$ values in the event. The y axis represents the ratio between the smallest and next to smallest z distance between a PV and the charged lepton. We could divide the x-y plane into four regions with a horizontal line and a vertical line. Their optimal positions can be decided by a future study. Events having at least one of the coordinates close to zero are events for which it is easy to identify the PV. However, events from the upper-right corner have PVs that present very close values for both the z positions and $\sum_{tracks} p_T$. For these events it is hard to choose the event PV and new algorithms must be developed. A non automatic solution to analyze these events

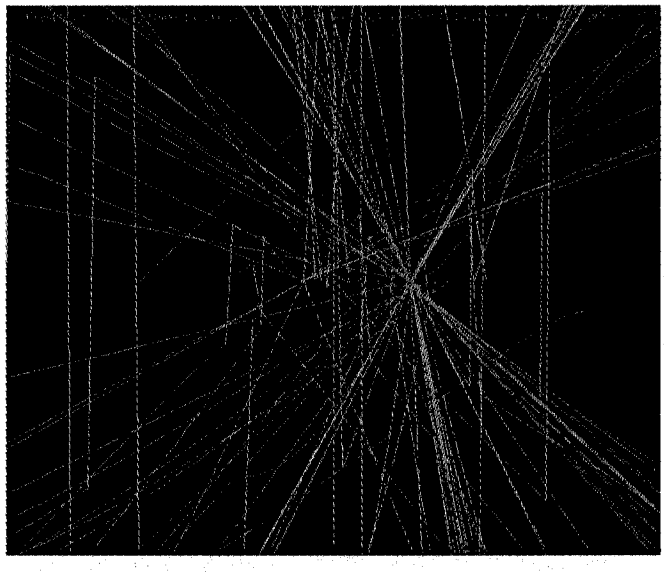

Figure 5–16: rz Event Display view of a MC event where tracking fails, leading to an unrealistically large value of $\sum_{tracks} p_T$ (PV_1: $z \approx 6$ cm and $\sum_{tracks} p_T \approx 55,000$ GeV). The correct event PV is therefore the PV closest in the z direction to the charged lepton (PV_2: $z \approx 31$ cm and $\sum_{tracks} p_T \approx 260$ GeV)

is that of using the CDF Event Display and understanding this way what is happening in these events.

5.5 Approach of DZero

Besides CDF, it is only the DZero Collaboration that also observes and studies real top-quark pair events. Therefore, they also need to find the best way to choose the event PV from the many PVs in the event, especially in the context of increasing instantaneous luminosity. Their approach is described in their public web page for the vertex algorithm group that deals with minimum bias events [58] and in a public note released by the DZero collaboration [59].

At Dzero, as at CDF, tracks originating from hard scatterings tend to have a larger transverse momentum than tracks originating from minimum bias events. Based on this, DZero builds an algorithm that gives the probability that a PV comes from a minimum bias interaction. After the algorithm is run on all the PVs in the event, the event PV is chosen as the one with the

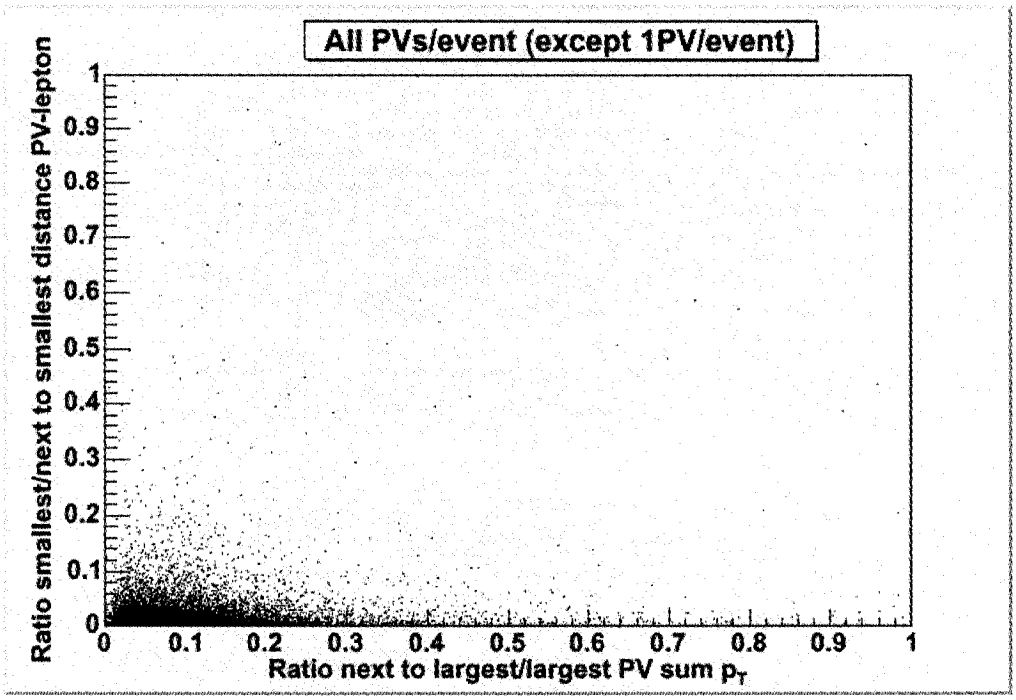

Figure 5–17: 2D histogram for events having at least 2 PVs: x-axis ratio next to largest and largest $\sum_{tracks} p_T$; y-axis smallest and next to smallest ratio of z distance between a PV and the charged lepton

minimum value of the probability to originate from a minimum bias interaction and therefore the maximum chance to originate from a hard scattering. However, as instantaneous luminosity increases the chance of obtaining more than one hard scattering in one event also increases and DZero needs to find new ways of choosing the event PV.

CHAPTER 6
Conclusions

6.1 Conclusions

In a given event, additional interactions affect the measurements for the wanted hard interaction. As instantaneous luminosity increases at CDF, CDF would face an increasing average PV multiplicity from 2 to 5 in the coming years. Studying a high luminosity minimum bias event $t\bar{t}$ signal Monte Carlo sample, we confirmed that the efficiency of choosing correctly the event PV for $t\bar{t}$ pair events in the lepton-plus-jets channel is above 99% for two algorithms of event PV selection: the most energetic PV in the event and the closest PV in the z direction to the charged lepton. However, the latter algorithm is more efficient for all values of PV multiplicity. We therefore confirm that CDF is currently using the proper algorithm and we recommend maintaining this algorithm as instantaneous luminosity increases or performing studies on new possible techniques, such as those proposed in this dissertation.

We also studied the square of the significance signal over background of the event PV charged lepton z distance cut over a wide range of possible cut values for various PV multiplicities on low luminosity samples currently used by CDF for analyses with 1 fb^{-1} of integrated luminosity data. We find a flat significance for all cut values larger than 1 cm for all PV multiplicities. We do not have enough sensitivity and are not able to recommend a particular cut value. It appears that any cut at a value larger than 1 cm is appropriate. We recall that the current cut value CDF uses is 5 cm. Since the background sources used in this analysis (W+jets) represent by far the largest source of backgrounds 4–1, we do not expect the result of this analysis to be changed if one took into consideration all the possible sources of background.

.

We emphasize that this study was performed in the context of $t\bar{t}$ event selection in the lepton-plus-jets channel. Other results may be found in other $t\bar{t}$ decay channels or for analyses with other final states. In particular, an improved understanding of the PV event selection performance is required in the W+jets signature, the most important background contribution for the $t\bar{t}$ signature.

Moreover, expertise gained both at CDF and DZero at the Tevatron in dealing with minimum bias interactions and their primary vertices will be very helpful for the ATLAS and CMS experiments at the Large Hadron Collider. At the Tevatron there are currently (in two years) on average 2 (5) hard interactions per event. At the LHC there would be on average 2 (25) hard interactions per event when LHC turns on (when LHC runs at designed luminosity).

6.2 Future Prospects

In this dissertation we performed a $t\bar{t}$ pair event PV selection study for events in the lepton-plus-jets decay channel where the charged lepton is a central electron. New studies would be able to test the current $t\bar{t}$ pair event PV selection criteria for events also in the lepton-plus-jets channel where the charged lepton is either a plug electron or a muon, in the dilepton or all-hadronic channels.

However, this study could also be performed for analyses that use a correct PV identification and study a wide variety of final state particles or signatures. Such analyses identify jets originating from a bottom quark, a charm quark or a tau lepton through the lifetime measurement technique. Also, analyses reconstructing jets also need correct event PV reconstruction in order to measure precisely the jet energies; these could benefit from a study of event PV selection efficiency. As CDF increases its instantaneous luminosity, this study will become more and more relevant.

Identifying the correct interesting event primary vertex from the many primary vertices in the event is a very necessary task. This task is hard for some final states at the Tevatron

and in general for all those at the Large Hadron Collider experiments. Studies and tools that would make this task easier are most welcome.

References

[1] W. Hollik, "Review: Status of the standard model", Talk given at International Workshop on Quantum Effects in the Minimal Supersymmetric Standard Model, Barcelona, Spain, 9-13 Sep 1997, e-Print Archive: hep-ph/9711492, unpublished.

[2] D. Treille, "Review of the standard model", Review talk given at the Conference: Rencontres de Moriond, Les Arcs, France, Mar 22-28, 1992, Published in Moriond 1992: Electroweak:0131-172

[3] Zurab Kakushadze, "A Brief review of three family grand unification in string theory", Talk given at 6th International Symposium on Particles, Strings and Cosmology (PASCOS 98), Boston, MA, 22-27 Mar 1998, Published in *Boston 1998, Particles, strings and cosmology* 556-566

[4] R.S. Chivukula, "Electroweak symmetry breaking", Prepared for 9th Mexican Workshop on Particles and Fields: Physics Beyond the Standard Model, Colima, Mexico, 17-22 Nov 2003, Published in J.Phys.Conf.Ser.37:28-33,2006

[5] L. A. Anchordoqui et al., "Probing Planck scale physics with IceCube", Published in Phys.Rev.D72:065019,2005

[6] Mariana Grana, "Flux compactifications in string theory: A Comprehensive review", Published in Phys.Rept.423:91-158,2006 e-Print Archive: hep-th/0509003

[7] J. Bernstein, "Spontaneous symmetry breaking, gauge theories, the higgs mechanism and all that", Published in Rev.Mod.Phys.46:7-48,1974

[8] J. Lopuszanski, "Some remarks on the higgs mechanism", Published in Fortsch.Phys.22:295-309,1974

[9] T. Hahn et al., "SM and MSSM Higgs Boson Production Cross Sections at the Tevatron and the LHC", (2006), e-Print Archive: hep-ph/0607308, unpublished

[10] An electronvolt (eV) is a non-SI energy unit and it represents the energy acquired by a particle charged with an elementary electric charge accelerated by an electric potential drop of a volt. Its multiples are used commonly to express energy, mass, time and space units in high energy physics.

[11] Xavier Calmet, Josep F. Oliver, "A Seesaw mechanism in the Higgs sector", (2006), e-Print Archive: hep-ph/0606209, unpublished

[12] R. Rattazzi, "Physics beyond the standard model", Prepared for EPS International Europhysics Conference on High Energy Physics (HEP-EPS 2005), Lisbon, Portugal, 21-27 Jul 2005, Published in PoS HEP2005:399,2006

[13] A. Morales, "Direct detection of WIMPs with conventional (non-cryogenic) detectors. Experimental review", Invited talk at 30^{th} International Meeting on Fundamental Physics (IMFP 2002), Jaca, (Huesca), Spain, 28 Jan - 1 Feb 2002, Published in Nucl.Phys.Proc.Suppl.114:39-57,2003

[14] Philippe Brax, Jerome Martin (Paris, Inst. Astrophys.), "Dark Energy and the MSSM", (2006), e-Print Archive: hep-th/0605228, unpublished

[15] L. Bellagamba, E. Sauvan, H. Spiesberger, "Electroweak physics and physics beyond the Standard Model", (2006), e-Print Archive: hep-ph/0607273, unpublished

[16] J. Erler, "Electroweak Physics at LHC", (2006), e-Print Archive: hep-ph/0607323, unpublished

[17] A. Palano, "Glueballs and hybrids: An Experimental review", High Energy Physics: QCD Workshop 94, Montpellier, France, 7-13 Jul 1994, Published in Nucl.Phys.Proc.Suppl.39BC:287-300,1995

[18] P. Jain, B. Kundu, H. Li , J. P. Ralston, J. Samuelsson, "A Review of pQCD calculations of electromagnetic form-factors of hadrons", Talk given at Workshop on the Structure of the Nucleon (NUCLEON 99), Frascati, Italy, 7-9 Jun 1999, Published in Nucl.Phys.A666:75-83,2000

[19] S. Muroya, A. Nakamura, Chiho Nonaka, T. Takaishi, "Lattice QCD at finite density: An Introductory review.", Published in Prog.Theor.Phys.110:615-668,2003

[20] H.Q. Ding, "Heavy quark potential in lattice QCD: A Review of recent progress", Published in Int.J.Mod.Phys.C2:637-658,1991

[21] I. Hinchliffe, "Quantum chromodynamics: in Review of Particle Physics (RPP 2000)", Published in Eur.Phys.J.C15:85-94,2000

[22] Bodo Lampe, "Top quark physics: A Popular review.", (1995), e-Print Archive: hep-ph/9512276, unpublished.

[23] Dhiman Chakraborty, Jacobo Konigsberg, David L. Rainwater, "Review of top quark physics", Published in Ann.Rev.Nucl.Part.Sci.53:301-351,2003

[24] U. Heintz, "Review of top quark physics", Prepared for 7^{th} Conference on Intersections Between Particle and Nuclear Physics (CIPANP 2000), Quebec City, Quebec, Canada, 22-28 May 2000, Published in AIP Conf.Proc.549:593-597,2002, Also in *Quebec City 2000, Intersections of particle and nuclear physics* 593-597

[25] Ming-Jer Wang, "Is there only top quark? Review of top results", To be published in the proceedings of Overseas Chinese Physics Association Conference on Recent Advances and Cross Century Outlooks in Physics, Atlanta, GA, 18-20 Mar 1999, Published in *Atlanta 1999, Recent advances and cross-century outlooks in physics* 101-112

[26] M. Narain, "Review of top quark physics: Present and future.", To be published proceedings of 4th International Conference on Hyperons, Charm and Beauty Hadrons, Valencia, Spain, 27-30 Jun 2000, Published in Nucl.Phys.Proc.Suppl.93:307-312,2001, Also in *Valencia 2000, Hyperons, charm and beauty hadrons* 307-312

[27] M. L. Mangano, T.G. Trippe, "The Top Quark: in Review of Particle Physics", Brief review in Eur.Phys.J.C3:1-794,1998, Published in Eur.Phys.J.C3:343-347,1998

[28] S. Eidelman et al., "Review of particle physics. Particle Data Group", Published in Phys.Lett.B592:1,2004

[29] R.D. Peccei, S. Peris, X. Zhang, "Nonstandard couplings of the top quark and precision measurements of the electroweak theory", Published in Nucl.Phys.B349:305-322,1991

[30] L.M. Lederman, "The discovery of the Upsilon, bottom quark, and B mesons", Given at 3rd International Symposium on the History of Particle Physics: The Rise of the Standard Model, Stanford, CA, 24-27 Jun 1992, unpublished

[31] F. Abe et al., " Evidence for top quark production in anti-p p collisions at s**(1/2) = 1.8-TeV", Published in Phys.Rev.Lett.73:225-231,1994

[32] F. Abe et al., "Evidence for top quark production in anti-p p collisions at s**(1/2) = 1.8-TeV", Published in Phys.Rev.D50:2966-3026,1994

[33] F. Abe et al., "Observation of top quark production in anti-p p collisions", Published in Phys.Rev.Lett.74:2626-2631,1995

[34] S. Abachi et al., "Observation of the top quark", Published in Phys.Rev.Lett.74:2632-2637,1995

[35] Public webpage of Top Quark Analyses of the Collider Detector at Fermilab Collaboration: http://www-cdf.fnal.gov/physics/new/top/top.html

[36] N. Kidonakis and R. Vogt, "Theoretical status of the top quark cross section", Presented at DPF 2004: Annual Meeting of the Division of Particles and Fields (DPF) of the American Physical Society (APS), Riverside, California, 26-31 Aug 2004, Published in Int.J.Mod.Phys.A20:3171,2005

[37] J. Alwall et al., "Is V(tb) $\approx$ 1?", e-Print Archive: hep-ph/0607115, unpublished; D. O'Neil et al. (ATLAS Collaboration), "Prospects for measuring V(tb) via s-channel single top at ATLAS", Published in J.Phys.G28:2657-2667,2002

[38] S.I. Alekhin, "Parton distribution functions from the precise NNLO QCD fit", Published in JETP Lett.82:628-631,2005, Pisma; S.I. Alekhin, "Comparative study of the uncertainties in parton distribution functions", Prepared for 8th International Workshop on Advanced Computing and Analysis Techniques in Physics Research (ACAT 2002), Moscow, Russia, 24-28 Jun 2002, Published in Nucl.Instrum.Meth.A502:761-763,2003

[39] V.G. Margoon, "Effect of superconductive destruction in YBa2Cu3O7-5 bulk bridges under the action of strong Joule self-heating", published in Journal of Superconductivity, v 9, n 1, Feb, 1996, p 129-134

[40] J. Marriner, "Stochastic cooling overview", Presented at International Workshop on Beam Cooling and Related Topics (COOL03), Mt. Fuji, Japan, 19-23 May 2003, published in Nucl.Instrum.Meth.A532:11-18,2004s

[41] D. Acosta et al., "The CDF Cherenkov luminosity monitor", Prepared for 8th Pisa Meeting on Advanced Detector: Frontier Detectors for Frontier Physics, La Biodola, Isola d'Elba, Italy, 21-25 May 2000, Published in Nucl.Instrum.Meth.A461:540-544,2001

[42] A. Abulencia et al., "Measurements of inclusive W and Z cross sections in p anti-p collisions at s**(1/2) = 1.96-TeV", e-Print Archive: hep-ex/0508029, Submitted to Phys.Rev.D

[43] D. Acosta et al., "Measurement of the t anti-t production cross section in p anti-p collisions at s**(1/2) = 1.96-TeV using lepton + jets events with secondary vertex b-tagging", Published in Phys.Rev.D71:052003,2005

[44] Carsten Rott, Daniela Bortoletto, "Primary Vertex Algorithm Comparison for High Pt Physics", CDF Internal NOte CDF/DOC/MISSING_ET/CDFR/6472 (2003), unpublished

[45] Kevin Burkett et al., "First Look At SecVtx Using Event Primary Vertex Finder PrimeVtx", CDF Public Note CDF/PUB/SEC_VTX/PUBLIC/6417 (2003), unpublished; Salvatore Rappoccio et al., " Impact of PrimeVtx on SecVtx For Summer 2003 Conference", CDF Internal Note CDF/PUB/SEC_VTX/PUBLIC/6666 (2003), unpublished

[46] Internal CDF website, top-quark group MC production webpage (password protected), http://www-cdf.fnal.gov/internal/physics/top/RunIIMC/topmc6/

[47] D. Abulencia et al., "Measurement of the $t\bar{t}$ Production Cross Section in $p\bar{p}$ Collisions at $\sqrt{s}$ = 1.96 TeV using Lepton+Jets Events with Jet Probability b-tagging", published in Phys. Rev. D74, 072006 (2006)

[48] D. Acosta et al., "The Underlying Event in Hard Interactions at the Tevatron p anti-p Collider", published in Phys. Rev. D70, 072002 (2004)

[49] Private communication with Rob Snihur

[50] Ayana Holloway et al., "First Direct Limit on the Top Quark Lifetime from CDF", CDF Public Note, submitted to ICHEP06, unpublished, http://www-cdf.fnal.gov/physics/new/top/confNotes/cdf8104_toplifepub.pdf

[51] Robin Erbacher et al., "Event Selection and $t\bar{t}$ Signal Acceptance of the Winter 2005 Top Lepton + Jets Sampe", CDF Internal Note CDF/ANAL/TOP/CDFR/7372 (2005), unpublished

[52] T. Sjostrand et al., "High-energy physics event generation with PYTHIA 6.1", Published in Comput.Phys.Commun.135:238-259,2001; T. Sjostrand, S. Mrenna, P. Skands, "PYTHIA 6.4 Physics and Manual", Published in JHEP 0605:026,2006

[53] P. Avery, K. Read, and G. Trahern, "QQ: A Monte Carlo Generator", Internal Software Note CSN-212, Cornell University, (1985), unpublished

[54] R. Brun, F. Carminati, "Simulation: Status and future trends for GEANT", Prepared for 9th International Conference on Computing in High-energy Physics (CHEP 91), Tsukuba, Japan, 11-15 Mar 1991, Published in *Tsukuba 1991, Computing in high energy physics* 451-458 ; R. Brun and F. Carminati, CERN Program Library Long Writeup W5013 (v3.14) (1993), unpublished

[55] E. Gerchtein, M. Paulini, "CDF detector simulation framework and performance", Talk given at 2003 Conference for Computing in High-Energy and Nuclear Physics (CHEP 03), La Jolla, California, 24-28 Mar 2003, Published in eConf C0303241:TUMT005,2003

[56] G. Corcella et al., "HERWIG 6.5 release note", CAVENDISH-HEP-02-17, DAMTP-2002-124, KEK-TH-850, MPI-PHT-2002-55, CERN-TH-2002-270, IPPP-02-58, MC-TH-2002-7, Oct 2002, 8pp, e-Print Archive: hep-ph/0210213, unpublished

[57] D.J. Lange, "The EvtGen particle decay simulation package", Prepared for Beauty-2000: 7th International Conference on B-Physics at Hadron Machines, Sea of Galilee, Kibbutz Maagan, Israel, 13-18 Sep 2000, Published in Nucl.Instrum.Meth.A462:152-155,2001

[58] Public webpage of Vertex Algorithm group of the DZero Collaboration at Fermilab: http://www-clued0.fnal.gov/~aran/d0work/mbpsel/how_to_use_PVSelect_MinBiasProb.html

[59] Ariel Schwartzman, Meenakshi Narain, "Probabilistic Primary Vertex Selection", DZero Public Note, (2002), unpublished, found at http://www-clued0.fnal.gov/~aran/d0work/mbpsel/do_note_4042.pdf